Fakultät für Medizin

Histopathological characterization of the impact of neoadjuvant therapy in human pancreatic cancer

Carmen Mota Reyes

Vollständiger Abdruck der von der Fakultät für Medizin der Technischen Universität München zur Erlangung des akademischen Grades eines

Doktors der Medizin (Dr. med)

genehmigten Dissertation.

Vorsitzender: Prof. Dr. Jürgen Schlegel

Prüfer der Dissertation:

1. Prof. Dr. Ihsan Ekin Demir, Ph.D.
2. Prof. Dr. Wilko Weichert
3. Prof. Dr. Roland M. Schmid

Die Dissertation wurde am 25.11.2020 bei der Technischen Universität München eingereicht und durch die Fakultät für Medizin am 08.06.2021 angenommen.

Dedicated to my mother, who fought her own battle against cancer and won.

“All humanity could be piled up on a small Pacific islet. The grown-ups, to be sure, will not believe you when you tell them that. They imagine that they fill a great deal of space. They fancy themselves as important as the baobabs. You should advise them, then, to make their own calculations. They adore figures, and that will please them."

Antoine de Saint Exupéry

from: The Littel Prince (1943), Chapter 17

Table of contents

Declaration on publication 6

Introduction 7

Pancreatic cancer: characteristics and clinical management 7

Neoadjuvant therapy in PCa 13

The tumor microenvironment in human PCa 15

PCa stroma: desmoplastic reaction, angiogenesis, neurogenesis and neural invasion 15

Role of immune cells in the PCa microenvironment 17

Aims of the study 22

Material & Methods 23

Laboratory expendable products 23

Reagents 23

Primary antibodies 24

Secondary antibodies 25

Selection of Patients 25

Immunhistochemistry (IHC) and immunofluorescence (IF) 27

Quantitative analysis 30

Desmoplastic reaction 30

Angiogenesis 31

Neurogenesis and NI 34

Tumor proliferation rate 36

Immune cell analysis....37
Statistical analysis....41
Results:....41
The tumor microenvironment of PCa after neoTx is characterized by reduced activation of the stroma and diminished NI....41
The angiogenesis and proliferation rate of tumor cells in PCa microenvironment remain constant after neoTx....44
Proinflammatory and anti-tumor immune cell populations are significantly increased in the PCa microenvironment after neoTx....46
The tumor infiltration by immunosuppressive cell subsets is significantly reduced after neoTx....49
Clinical impact of the histopathological features of PCa microenvironment on survival....51
Discussion....54
Conclusion....63
References....64
Acknowledgments....71

Declaration on publication

Part of the results presented in this dissertation have been published as follows:

Journal: Clinical Cancer Research

Title: Neoadjuvant therapy remodels the pancreatic cancer microenvironment via depletion of pro-tumorigenic immune cells

Authors: Carmen Mota Reyes, Steffen Teller, Alexander Muckenhuber, Björn Konukiewitz, Okan Safak,Wilko Weichert, Helmut Friess, Guralp Ceyhan, and Ihsan Ekin Demir

Date: September 4, 2019

doi: 10.1158/1078-0432.CCR-19-1864

Introduction

Pancreatic cancer: characteristics and clinical management

Pancreatic cancer (PCa) is one of the deadliest human neoplasms and its dismal prognosis has remained virtually unchanged over the past decades (1). PCa continues to rank fourth among the cancer-associated deaths in the U.S.A. and it is predicted to be the second leading cause of cancer-related deaths by 2030 in Western countries (1, 2). The 5-year overall survival rate is reported to be around 5%, with almost all survivors belonging to the 20% of patients, who present with resectable disease; for these patients, the 5 year survival rate is 15-25% (1). This dismal prognosis is a result of the late diagnosis of the disease, the lack of biomarkers, the early metastatic dissemination as well as the resistance to systemic therapies (3, 4).

PCa evolves through non-invasive precursors lesions, mostly pancreatic intraepithelial neoplasia (PanIN) (5), acquiring clonally selected genetic and epigenetic alterations along the way (6). It shows a distinctive pattern of genetic alterations involving the activation of K-RAS oncogene, the inactivation of tumor-suppressor genes including p16/CDKN2A, TP53, BRCA2 and MADH4/SMAD4/DPC4, widespread chromosomal losses, gene amplifications and telomere shortening (2, 6-8). These alterations occur at different stages of the disease, which suggests that an accumulation of multistep genetic alterations takes place in the development of PCa (9-11). The earliest genetic abnormalities are KRAS mutations and telomere shortening, which are even present in low-grade pancreatic PanIN, whereas the inactivation of TP53, SMAD4 and BRCA2 are only recorded in advanced PanIN and invasive carcinomas (8) (Figure 1). The presence of multiple genetic mutations in PCa patients correlates with worsened prognosis and shortened survival (11) (Figure 1).

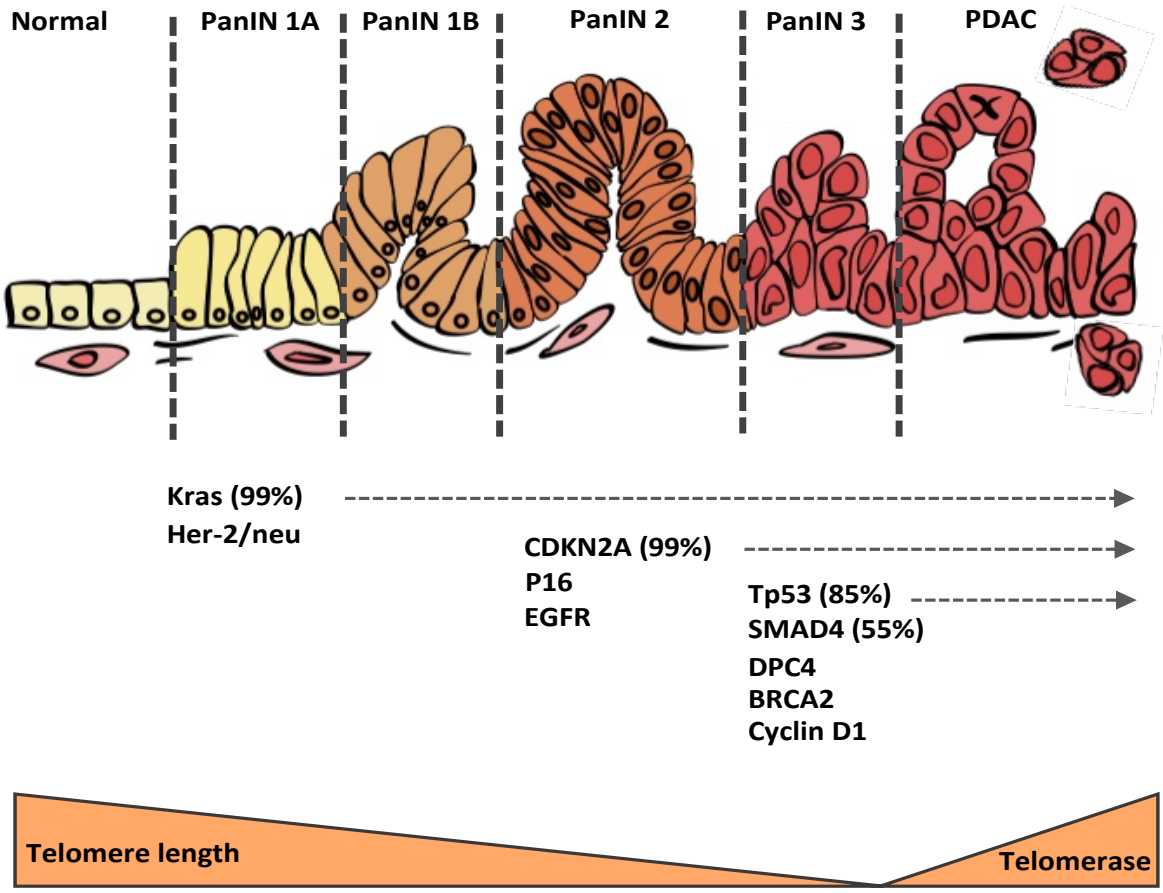

Figure 1. PanIN progression model of PCa related to genetic alterations. The sequential accumulation of mutations in PCa-driving genes accounts for the emergence of invasive PCa from the normal epithelium over PanIN lesions. Image adapted from Fig 1. in "Progression Model for Pancreatic Cancer" (12)

One of the major challenges to detect PCa is its late clinical presentation, with nearly all symptomatic patients having an advanced disease (2). PCa often progresses asymptomatically and when it does present, clinical manifestations are non-specific and include abdominal pain, asthenia, jaundice, unexplained weight loss, new-onset diabetes mellitus and, rarely, migratory thrombophlebitis (1, 3, 11, 13). Risk factors such as cigarette smoking, type 2 diabetes mellitus and chronic pancreatitis are related to approximately one quarter of the cases (1) (Figure 4).

In the past years, a great deal of research has been invested in the identification of reliable diagnostic biomarkers of PCa to allow early screening, since the widely used, CA19-9 lacks sufficient sensitivity or specificity to be used as early diagnostic marker

(1). However, it is routinely used to monitor disease progression, recurrence and therapy response (1, 2). The detection of circulating tumor DNA encoding mutant KRAS or TP53 as well as the presence of increased circulating branched chain amino acids indicating tissue protein breakdown, have been proven successful in PCa GEMMs and in some patients up to 5 years before the diagnosis and could serve as non-invasive early diagnostic tests (1).

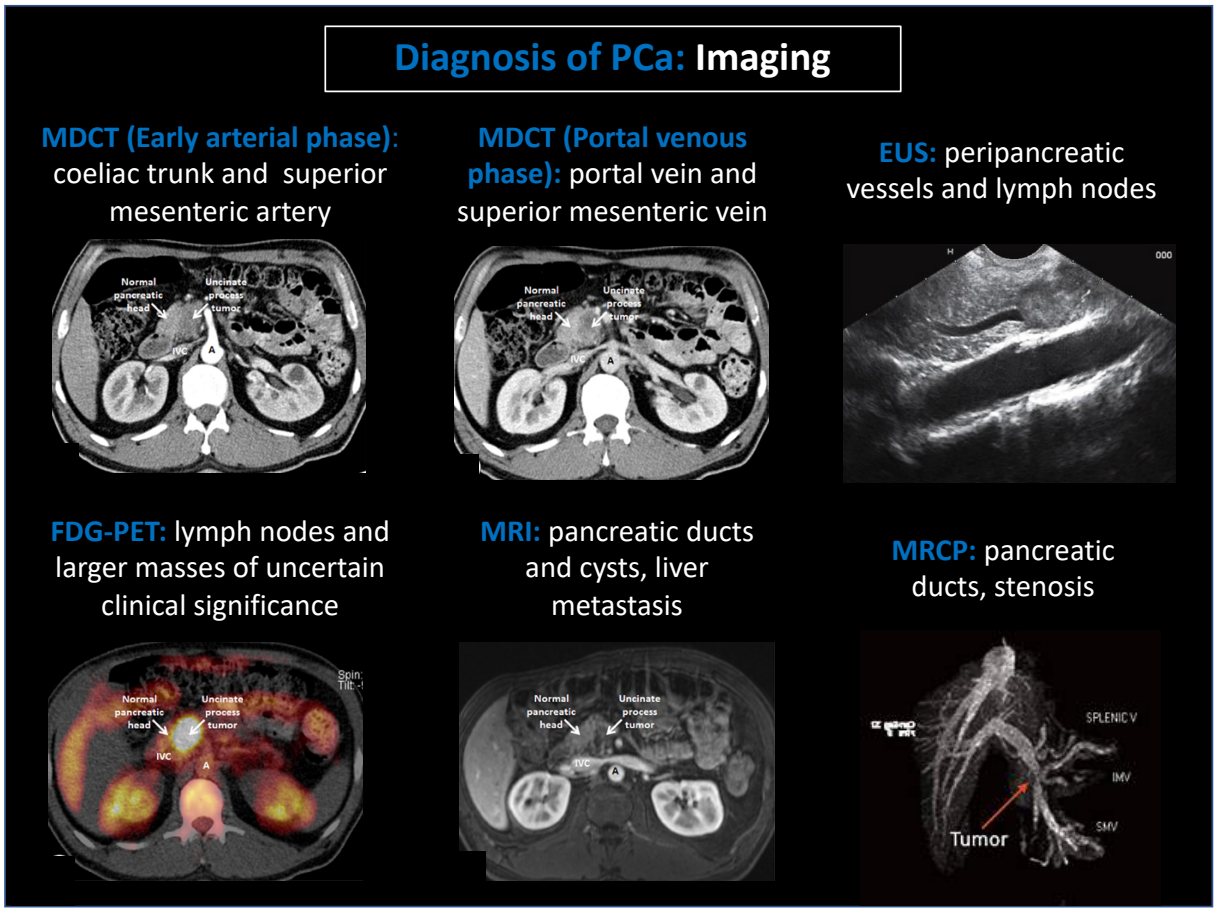

Figure 2. Imaging modalities in the diagnosis of PCa. The specific utility of each modality is shown in white next to its name. MDCT: multidetector computed tomography, FDG-PET: fluorodeoxyglucose positron emission tomography(14), MRI: magnetic resonance imaging(14), EUS: endoscopic ultrasound(15), MRCP: magnetic resonance cholangiopancreatography. MDCT, FDG-PET and MRI images were taken from "How fibrosis influences imaging and surgical decisions in pancreatic cancer" (Erkan et al 2011); EUS image was found on "Role of endoscopic ultrasound in idiopathic acute pancreatitis with negative ultrasound, computed tomography, and magnetic resonance cholangiopancreatography" (Rana et al 2012); MRCP image was taken from the website "https://www.pancan.org/facing-pancreatic-cancer/diagnosis/magnetic-resonance-imaging-mri/)" from the pancreatic cancer action network.

The diagnosis of PCa requires a combination of radiological imaging and endoscopic procedures (3). Triple-phase-multidetector CT (MD-CT) provides excellent resolution of the pancreas and surrounding vasculature and is the current gold standard to

evaluate the resectability the tumor (3, 11). Contrast-enhanced magnetic resonance imaging (MRI) and endoscopic ultrasonography (EUS) and their combinations with nuclear imaging, e.g. 18F-Desoxyglucose (FDG) positron emission tomography (PET) can be used to improve diagnostic accuracy (3, 11, 16) (Figure 2).

Cancer staging subsequently follows, with the American Joint Committee on Cancer providing the standard model based upon the tumor-node-metastasis (TNM) system. As a result, PCa patients can often be classified into three major cohorts (11, 17) (Figure 3):

- Resectable tumor
- Borderline resectable tumor or locally advanced disease: localized tumors with high risk for margin-positive resection when treated primarly with surgery
- Sistemically disseminated metastatic disease

TNM Staging	Anatomic stage / Prognostic groups
T1	Tumor 2 cm or less
	T1a Tumor 0.5 cm or less
	T1b Tumor greater than 0.5 cm and less than 1 cm
	T1c Tumor greater than 1 cm but no more than 2 cm
T2	Tumor more than 2 cm but no more than 4 cm
T3	Tumor more than 4 cm in greatest dimension
T4	Tumor involves coeliac axis, superior mesenteric artery and/or common hepatic artery
N1	Metastases in 1 to 3 nodes
N2	Metastases in 4 or more nodes
M0	No distant metastasis
M1	Distant metastasis

Figure 3. AJCC 8th Edition Staging. American Joint Commitee on Cancer.

Due to its late diagnosis, the majority of patients present with metastatic dissemination or locally advanced disease, precluding them from resection (2, 11). Only 20% of PCa patients are candidates for curative surgical resection by the time of diagnosis (2). Depending on the localization of the tumor, the type of operation would be classical or pylorus-preserving (pp) pancreaticoduodenectomy (Whipple's operation) for

pancreatic head tumors, total pancreatectomy for tumors of the body, and distal pancreatectomy for tail tumors (2, 11). Given that surgery alone is not sufficient to achieve long-term survival, adjuvant therapy is standard following tumor resection (1). Postoperative therapy with either gemcitabine or mFOLFIRINOX (a combination of oxaliplatin, irinotecan and leucovorin) has demonstrated significant survival benefit and is the standard treatment (1). For those patients who undergo resection, the prognosis remains poor owing to the high rate of local recurrence and distant metastasis (18) (Figure 4).

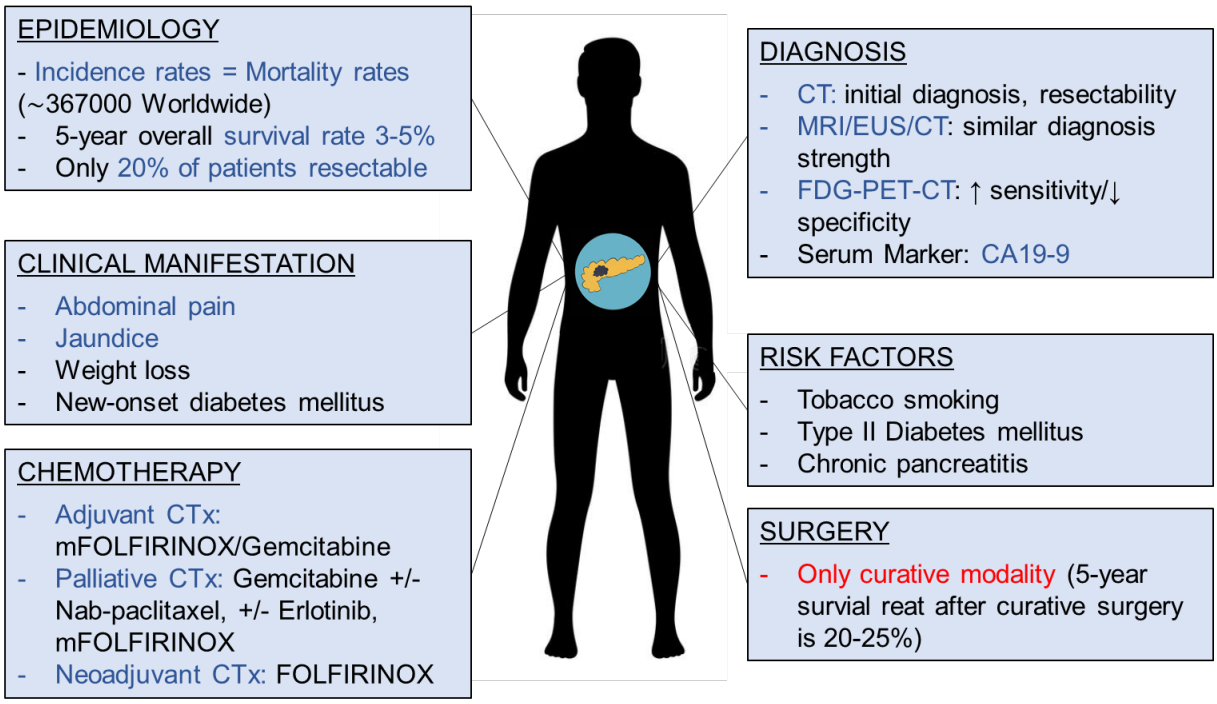

Figure 4. The defining features of human PCa from a clinical perspective.

Surgical resection remains the only potentially curative modality for PCa (6, 19), 30-40% of the initially unresectable patients, however, present with a locally advanced/borderline resectable tumor without systemic dissemination. In order to downstage the tumor and enable its resection, neoadjuvant approaches are currently being tested in randomized trials. Patients with metastatic dissemination qualify only for palliative treatment and gemcitabine +/- erlotinib has been the standard of care for

many years, which marginally extended survival rates on approximately one month. Recently, two novel combination chemotherapies have considerably improved the median survival in metastasized PCa patients, the gemcitabine-free, FOLFIRINOX (FOLFIRINOX with 5-fluororacil) regimen and the combination of gemcitabine with nab-paclitaxel. However, the efficacy of these treatments is not satisfactory in the broader sense, with a median survival of 6.8 to 11.1 months (2, 4) (Figure 5). The reason for the distinctive PCa resistance to chemotherapeutical approaches could be partly explained by the diverse influences exerted by the microenvironment. Intriguingly, there is a high discrepancy between the relative success of therapies such as gemcitabine, reported in preclinical assays, and the subsequent failure in human PCa (4). Therefore, shedding light on the underlying molecular mechanisms of cross-talk between tumor cells and other elements of the tumor microenvironment remains one of the biggest challenges to finally overcome the dismal prognosis of PCa (4).

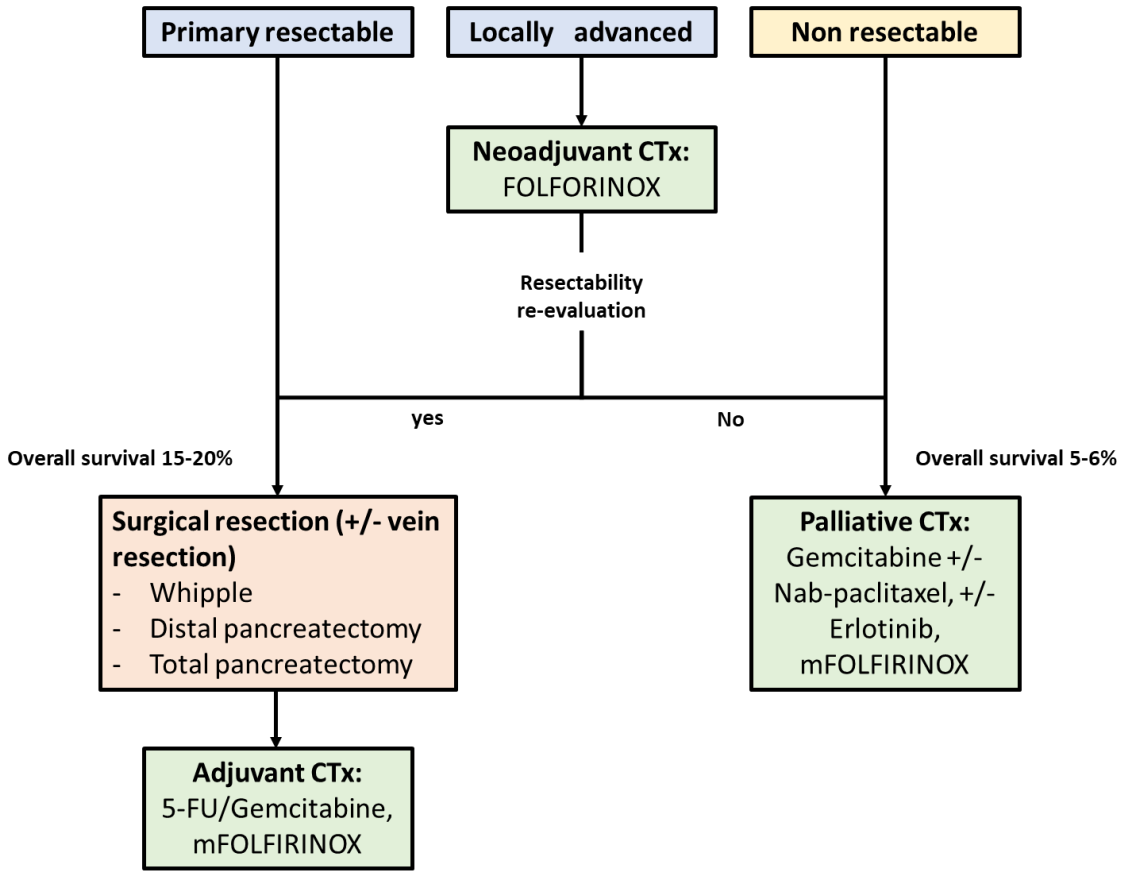

Figure 5. Flowchart for the treatment of PCa

Neoadjuvant therapy in PCa

Neoadjuvant therapy (neoTx) has become the standard of care for many gastrointestinal malignancies: randomized trials have demonstrated beneficial effects for oesophageal, gastric and rectal cancer (2). Considering these findings from other gastrointestinal cancers, the introduction of neoTx for PCa appears reasonable and has gained massive popularity over the past 20 years (20). This treatment has a strong rationale and many theoretical advantages endorsed by the National Comprehensive Cancer Network (NCCN) guidelines (2, 21).

Rationale for preoperative Neoadjuvant Chemotherapy (NCCN)

- **Tumor downstaging**
- Early treatment of **micrometastatic lesions**
- Upfront treatment with **higher compliance** and **improved dose-intensity**
- **Reducing the risk of R1 resection** and peritoneal implantation during operation
- Assesment of **tumor chemosensitivivity in vivo** and **avoidance of surgical morbidity**

For borderline resectable and locally advanced PCa, there is evidence that neoTx increases the probability of negative resection margins and the number of patients who can undergo surgery. On the other hand, for resectable PCa, neoadjuvant chemotherapy or chemoradiation remains debatable because of the conflicting data on its effectiveness, and because there is no phase III trial to support their use (19).

Resectability is based on the extent of vascular involvement and is usually determined using a combination of imaging tests and laparoscopic assessment of the peritoneal cavity to rule out small peritoneal metastases whose detection might be missed in CT or MRI scans (19) (Table 1). In the past decade, the surgical attitude towards PCa has dramatically changed, patients with arterial or venous tumor involvement, who not so

long ago were considered irresectable, are now candidates for surgical resection under certain instances (19, 20).

TNM Staging	Clinical staging	NCCN Criteria of defining resectability
0 Tis N_0 M_0	**Resectable**	No extension into regional arteries (CA,CHA,SMA) or veins (SMV, PV). PV extension to <180°
IA T_1 N_0 M_0		
IB T_2 N_0 M_0		
IIA T_3 N_0 M_0		
IIB T_{1-3} N_1 M_0		
III T_4 N_{1-2} M_0	**Borderline resectable/ locally advanced**	**Borderline resectable**: solid tumor contact with: - CHA/SMA <180° - CA <180° or >180° with inert aorta and gastroduodenal artery - SMV/PV >180° or <180°with contour irregularity/thrombosis permitting safe reconstruction **Locally advanced** (technically irresectable without disseminated dieease) - CA/SMA >180° - CA and aorta engrossment - 1st duodenal branch of SMA - Proximal jejunal draining into SMV - Tumor involvement or occlusion of SMV/PV rendering it unreconstructible
IV T_{1-4} N_{1-2} M_1	**Unresectable**	**Distant metastasis**

Table 1. Classification of PCa upon TNM Staging, clinical resectability and NCCN Critaria for resectability. CA: celiac artery, CHA: common hepatic artery, PV: portal vein, SMA: superior mesenteric artery, SMV: superior mesenteric vein (19)

Unresectability used to trigger palliative treatment in the past, since cure was considered impossible. However, secondary resectability can also be achieved in such advanced tumors after neoadjuvant (radio-)CTx regimen. Results for regimens such as FOLFIRINOX (22) are encouraging and suggest that the R0-resection and survival rates achieved after such a neoadjuvant approach are similar to those after primary tumor resection (20, 23). The current trend in the preoperative management of locally

advanced PCa is towards randomized controlled trials addressing ongoing issues such as (17):

- Optimal timing of surgery i.e. neoTx vs upfront surgery for both resectable and borderline resectable pancreatic cancer (NEONAX-Study - AIO-PAK-0313**)**
- Optimal chemotherapy regimen in the neoadjuvant setting (e.g. FOLFIRINOX vs gemcitabine/nab-paclitaxel vs. added radiation)
- Potential benefit of various immunotherapy regimes and cancer vaccines

The tumor microenvironment in human PCa

The tumor microenvironment, comprising multiple cellular and molecular factors, has arisen as an integral part for the initiation, growth and progression of PCa (24, 25).

PCa stroma: desmoplastic reaction, angiogenesis, neurogenesis and neural invasion

The presence of a strong desmoplastic reaction is a pathognomonic feature of PCa and has been widely reported to promote tumor progression, metastasis and chemoresistance (26-28). Activated PSCs are the main orchestrators and producers of this abundant extracellular matrix (26, 27) composed of proteins such as collagens, fibronectin and laminin, as well as non-collagenous proteins like glycoproteins, proteoglycans and glycosaminoglycans (1). The cellular components of the stroma comprise PSCs, infiltrating immune cells, endothelial and neuronal cells (1, 29, 30). Whether the extent of stromal activation influences the clinical outcome of PCa patients remains controversial. A large study including 233 patients showed that the number of activated PSCs was associated with poor clinical outcome; however, this finding was not corroborated by two subsequent studies (1). A recent study showed that multimodal neoTx was able to decrease the activation of the stroma; however, the effects of chemotherapeutical agents on pancreatic stroma are not entirely understood

and still debatable (31). Furthermore, growing evidence pointed out a possible immunomodulatory role of PSCs by sequestration of $CD8^+$ T cells away from cancer cells and the promotion of the migration of myeloid derived suppresor cells (MDSC) into the stroma, which suppressed tumor immune-surveillance (26, 32, 33).

Although both cancer and PSCs secrete proangiogenic factors (VEGF, basic fibroblast growth factor and periostin), PCa is a scirrhous and hypoxic tumor, where the majority of its capillaries and lymphatic vessels collapsed because of high interstitial pressure (27, 34) and therefore results in impaired drug delivery (35). Angiogenesis has been associated with disease progression in many solid malignancies, however the statement that tumors need angiogenesis to grow, invade and metastasize seems no longer applicable to all tumors (36). In fact, due to its reduced microvascular density, PCa has been suggested as an example in which angiogenesis is less essential for tumor progression (35, 36). The hypoxic environment within the tumor leads to the expression of certain hypoxia inducible factors (HIF) and VEGF that contribute to the recruitment of several immunosuppressive cells such as MDSCs, M2 macrophages and regulatory T cells (Treg) (35). Endothelial cells have also been identified as pivotal regulators of immune cell trafficking, being able to induce apoptosis selectively in $CD8^+$ T cells but not in $CD4^+$ Tregs during the process of extravasation (27). Furthermore, hypoxia might act as a physiological selective agent against apoptosis-competent cells in tumors, thus promoting the clonal expansion of cells that acquire mutations in their apoptotic programs (36)

As the tumor progresses, intrapancreatic nerves undergo prominent plastic alterations, including increased neural density, hypertrophy, and neuritis (37, 38). However, the most prominent feature of pancreatic neuropathy in PCa remains the invasion of tumor cells to the nerves within the pancreas and the peripheral peri- and retropancreatic

nerve plexus (37, 38). NI is a phenomenon in which cancer cells invade the space surrounding nerves, penetrating the perineurium and becoming intimately associated with Schwann cells and axons in the endoneurium, which provides an alternative route for metastatic spread and pain generation (39). NI is encountered in nearly 100% of the PCa patients and its severity is thought to be an indicator of aggressive tumor behaviour. NI has been shown to correlate with local recurrence and shortened survival (39-41). In contrast to previous assumptions, NI is not simply the passive movement of tumor cells along the path of least resistance, but a directed process that involves many signalling molecules from various signalling pathways building a mutual chemoattractive gradient between nerves and cancer cells (37). Specific therapeutic approaches targeting NI in PCa in the clinical setting are largely lacking.

Ki67 is a nuclear protein, which has been widely used as proliferation marker in many solid malignancies (42). In lung and prostate cancer, it has been reported to be a prognostic marker (43, 44). Mixed results have been reported regarding PCa: ki67 expression has been reported to correlate with pathological grade, lymph node metastasis, recurrence and clinical stage (45). Stanton et al, however, showed no correlation of tumor proliferation rate with survival (46). In order to determine the potential of ki67 to predict therapy response and clinical outcome, we decided to include this histopathological feature in our analysis.

Role of immune cells in the PCa microenvironment

The immune system is one of the major modulators of tumor development and progression, and the crosstalk between immune cells and cancer cells has arisen as a novel hallmark of cancer (47). In PCa, the host immune surveillance represents the first filter to identify and eliminate malignant cells; however, throughout carcinogenesis, tumor cells develop numerous strategies to avoid recognition by the host immune

system, allowing them to escape from immune control and continue cancer progression (47). Even in its early stages, the tumor microenvironment has a highly immunosuppressive composition comprising increased numbers of alternatively activated tumor-associated macrophages (TAM) with an M2 phenotype, Treg cells as well as MDSCs (48-50). Together, they reduce the anti-tumor functionality and thus result in an impairment of tumor recognition and elimination.

Tumor infiltrating $CD8^+$ T cells are the most prevalent T cell population in PCa; they constitute primarly cytotoxic effector cells with the ability to lyse target cells (50). PCa cells, however, have the ability to render cytotoxic T cells anergic by PD-L1 expression and evade antigen recognition by losing the expression of MHC class I (50). In ovarian and colorectal cancers, among other malignancies, high levels of intratumoral $CD8^+$ T cells constitute a favourable prognostic factor (24, 51, 52) and the possibility of restoration of their effector role represents one of the main objectives of novel targeted therapies (53). $CD4^+$ T cells activate innate immune cells and modulate the function of B cells and $CD8^+$ T cells through cytokine secretion and direct cell–cell signalling (50). In the immunosuppresive microenvironment of PCa, secreted cytokines like interleukin (IL) 10, IL4 and IL13 skew the polarization of $CD4^+$ T cells to a protumorigenic Th2 phenotype, which have been correlated with reduced survival. Dendritic cells (DC) have been postulated as the most potent antigen-presenting cells and play a crucial part in the initiation, programming and regulation of antitumor immunity, directing cytotoxic T lymphocytes and NK cells to become potent antitumor effectors capable of eradicating malignant cells (54). NK cells are members of the innate immune response and mediate a direct elimination of tumor cells without prior sensitization (50). The numbers of circulating NK cells are diminished in cases of advanced PCa and

pretreatment levels of peripheral NK cells positively correlate with the overall survival of PCa patients (50).

Derived from the host's monocytes, we can distinguish in the tumor microenvironment TAMs and MDSCs. Macrophages are normally responsible for clearing debris from sites of injury or infection, and they also present antigens to the host's B and T cells to trigger adaptive immunity (55). TAMs can be polarized by IFN-gamma and IL-12 into inflammatory M1-type macrophages; however, the hypoxic environment of pancreatic tumors and cytokines like IL-4, IL-10 and IL-13 promote arginase-producing immunosuppressive M2 polarization (50). The elevated fraction of M2-polarized TAMs was reported to correlate with an increased risk of lymph node metastasis, NI, chemoresistance, worsening prognosis, and survival (56, 57). The ability of M2-TAMs to enhance tumor invasion and metastasis is not only by preventing tumor cells from being eliminated by $CD8^+$ cytotoxic T cells, but also by promoting matrix remodelling and angiogenesis, stimulating extracellular matrix breakdown, and augmenting epithelial-mesenchymal transition (EMT) (50). MDSCs, on the other hand, are a heterogeneous population of immature myeloid cells that have a critical role in the tumor microenvironment through immunosuppression (53). They have been implicated in the progression of breast cancer, melanoma and colon cancer, but their role in PCa has yet not been well defined (55). Granulocyte macrophage colony-stimulating factor (GM-CSF) promotes recruitment of myeloid progenitor cells to the surrounding stroma and subsequent differentiation into MDSCs. MDSCs suppress T cells through multiple mechanisms such as depletion of L-arginine, use of reactive oxygen species (ROS) or free radical peroxynitrate, and down-regulation of L-selectin. MDSCs can also sequester cysteine that is required for T cell activation (50). Furthermore, MDSCs are able to expand immunosuppressive Tregs through the secretion of transforming growth

factor β (TGF-β) and interferon (IFN)-gamma dependent secretion of IL-10 and impede innate immunity by conversion of macrophages to M2 phenotype and suppression of NK cells (50). Owing to their versatile immunosuppression, MDSCs represent an appealing but elusive potential therapeutic target. Surprisingly, the current standard chemotherapy for PCa, gemcitabine, has been unknowingly targeting MDSC and increasing antitumor response (58). Although limited in success so far, these early studies all show that targeting various components of MDSCs like colony stimulating factor 1 receptor (CSF1R), programmed death-ligand 1 (PD-L1) and cytotoxic T lymphocyte-associated protein 4 (CTLA4), may have a promising future in the treatment of PCa (50).

Although Tregs are critical for the maintenance of immunological self-tolerance, they also have the ability to impede the anti-tumor immune response in a variety of cancer types (50, 59). Even on preinvasive stages, PCa presents a pronounce infiltration of Tregs in the tumor microenvironment, which progressively increases as the tumor progresses (60). A high frequency of Tregs in the pre-neoplastic pancreas correlates with decreased survival in human PCa (60). A variety of mechanisms for Treg cell-mediated suppression of effector T cell responses have been proposed, including direct elimination of effector T cells and competition with effector T cells for access to antigen-presenting DCs, favouring tumor growth (60). The immune-inhibitory modes ascribed to Tregs involve the secretion of suppressive cytokines such as IL10, CTLA-4, and TGFβ (61, 62). Since Tregs are abundant and may suppress antitumor immune responses in PCa, Tregs are an appealing target for immune therapy. The role of tumor infiltrating B cells in relation to the tumors is controversial. Recent studies demonstrated that B cells are involved in the progression of PCa through a subset of B cells able to suppress the antitumor immune responses (50). The protumorigenic

effect B cells is mediated by IL-35 expression, which enhances the proliferation of PCa cells (50, 63). Furthermore, recent evidence suggests that B cells induce the M2-macrophage phenotype (50).

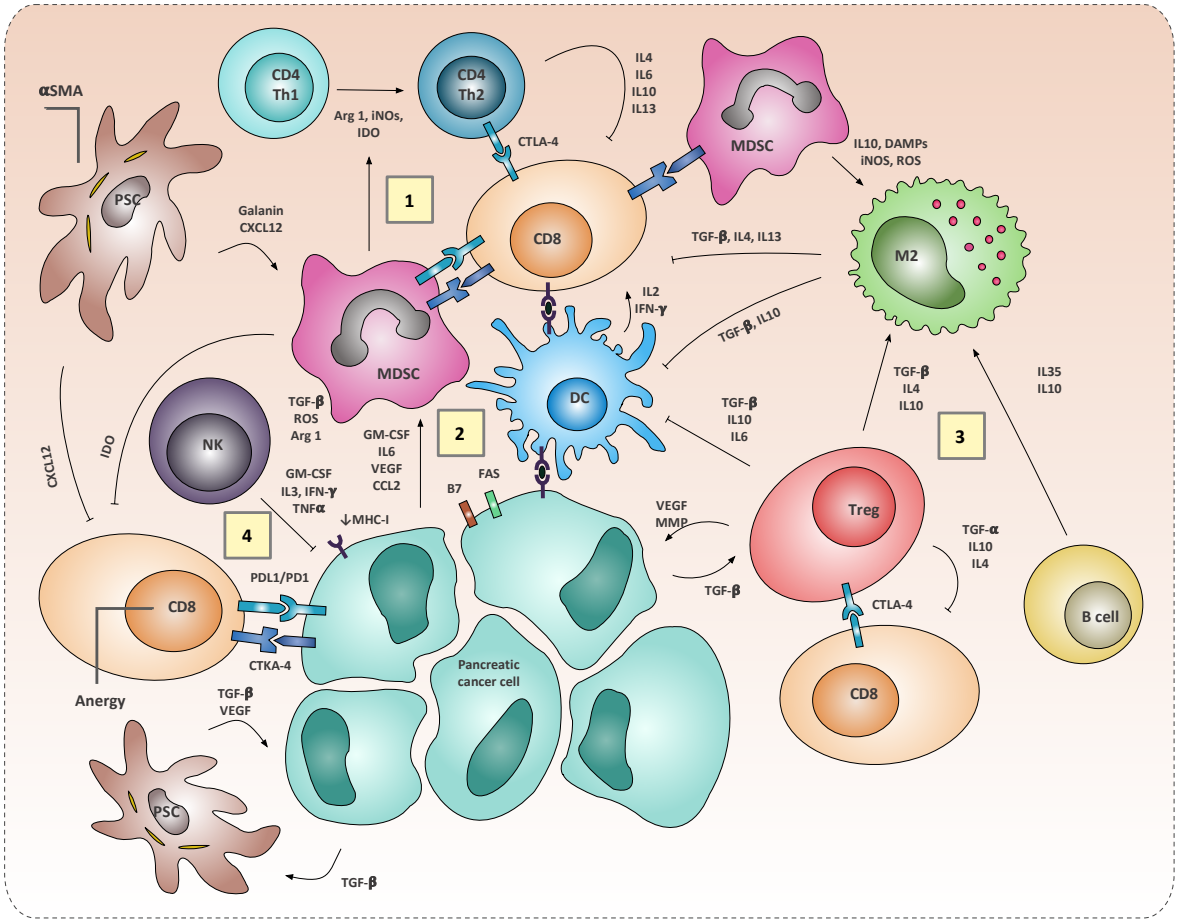

Figure 6. The PCa-mediated immunosuppressive tumor microenvironment. **(1)** PCa inhibit the proliferation and migration of $CD4^+$ T cells in the vicinity of the tumor. Furthermore, cytokines like IL10 and TGF-β contribute towards the polarization to Th2 phenotype with further tumor-promoting effects (50). **(2).** Tumor derived GM-CSF has been suggested to recruit and contribute to the differentiation of the highly immunosuppressive MDSCs, which suppress $CD8^+$ T cells (via depletion of L-arginin, use of ROS or starving them from tryptophan through the IDO (indoleamine 2,3-dioxygenase) and expand Tregs and M2 macrophages (50). **(3)** Cytokines like IL4, IL10 and IL13 from the tumor and protumorigenic immune cells induce the M2-polarization of macrophages. These cells are able to enhance tumor invasion and metastasis and are able to render $CD8^+$ T cells and NK cells anergic by the secretion of PD-L1 (50). **(4)** PSCs exhibit increased proliferation, expression of matrix metaloproteinases (MMPs) and fibronectin synthesis. Additionally, PSCs contribute to immune evasion by sequestering cytotoxic T cells in the stroma (via CXCL12 secretion), preventing them from invading peritumoral regions. Cancer cells mediate impairment of $CD8^+$ T cells cytolytic functions by expression of PD-L1 and CTLA-4, which bind to PD-1 and CTLA-4 receptor, respectively, on T cells and lead to cell anergy (26, 32, 64). Tregs infiltrate adjacent to PCa tissue due to the tumoral secretion of TGF-β, express CTLA-4 and are able to secrete of IL-6, IL10 and TGF-β, which further suppress the activity of $CD4^+$ and $CD8^+$ T cells, M1 macrophages, NK cells and DCs (50, 60). B cells induce the protumorigenic macrophage phenotype and stimulate the proliferation of PCa cells by IL35 expression (65).

The possibility to re-educate the immune response through neoTx is tempting. Shibuya et al. already demonstrated that neoTx attenuated the infiltration of Tregs and myeloid

cells in PCa; likewise, successful multimodal perioperative therapy was able to alter the immunomodulatory balance on breast and oesophageal tumors and was associated with increased infiltration of both $CD4^+$ and $CD8^+$ T cells (66, 67). These findings strongly suggest that the presence of an antitumoral immune response induced by neoTx could restrain tumor growth and reduce cancer aggressiveness and highlights the urgent need for new therapeutic strategies, especially immunotherapy (68). Targeted therapies against immunosuppressive cells such as GVAX (granulocyte-macrophage colony stimulating factor gene-transfected tumor cell vaccine) or agonistic CD40 lack any survival benefit in preclinical settings; however, promising results are rising in combination with immune-checkpoint blockade therapies (anti PD-1, -PD-L1 or -CTLA4) that enhance the antitumor activity of endogenous T cells. To reach a clinical benefit, however, a greater understanding of the dynamic immune composition of PCa is fundamental (33). Despite the high amount of research regarding the interaction and molecular crosstalk between immune cells and tumor cells, a comprehensive analysis of the influence of neoTx on the most important immune cell types in the PCa microenvironment has yet not been performed.

Aims of the study

The crucial role of the tumor microenvironment, and in particular of the immune system in the modulation of tumor progression and response to therapy has recently become clear. Multiple conventional chemotherapeutics and some targeted anticancer agents routinely used in patients affected by solid tumors, as well as selected forms of radiotherapy, have been shown to mediate robust immunostimulatory effects that are relevant for therapeutic responses (66, 67). We hypothesized that successful multimodal neoTx is accompanied by alterations in the local immune response that might serve to tip the balance in favour of antitumor immunity.

In the present study, we conducted a comprehensive histopathological characterization of the tumor microenvironment in neoadjuvantly treated PCa patients vs. primarly resected patients. For this purpose, a variety of immunohistochemical and immunofluorescence stainings were performed to analyze all distinctive histological features of human PCa, including:

- Stromal components: desmoplastic reaction, pancreatic neuropathy and neural invasion and angiogenesis
- Tumor proliferation rate
- Immunological response: cytotoxic T lymphocytes, B lymphocytes, Tregs, MDSCs, DCs, macrophages (M1 and M2) and NK cells

Finally, we correlated the results of the histopathological analysis with the clinical variables of our patients.

Material & Methods

Laboratory expendable products

Product	Company	Country
R.T.U. Normal Horse Serum (2,5%)	VectaMount	Burlingame, U.S.A
Normal goat Serum (10%) (NGS)	Invitrogen	California, U.S.A.
Aqua destillata	Braun	Melsung, Germany
Permanent Mounting Medium	VectaMount	Eching, Germany
Fluorescence Mounting medium	DAKO	Hamburg, Germany
Superfrost Menzel-Gläser Slides	Thermo Scientific	Regensburg, Germany
Coverslips 22x40mm	Thermo Scientific	Regensburg, Germany
Pipette tips	Star Lab	Ahrensburg, Germany
Pipetts	Eppendorf	Wesseling-Erzdorf, Germany
Falcon Tubes 15ml and 50ml	Greiner	Frickenhausen, Germany
Reaction tubes (1,5ml)	Eppendorf	Wesseling-Erzdorf, Germany

Reagents

Product	Company	Country

Liquid DAB+ Substrate Chromogen System	DAKO	Hamburg, Germany
Bouin´s solution	Sigma Aldrich	Missouri, U.S.A.
Weigert´s iron hematoxylin solution	Merck	Darmstadt, Germany
Phosphotungstig/Phosphomolybdic acid	Merck	Darmstadt, Germany
Acetic Acid solution	Carl Roth GmbH	Karlsruhe, Germany
Anilin blue	Merck	Darmstadt, Germany
EDTA buffer solution	Sigma Aldrich	Missouri, U.S.A.
Tris	Carl Roth GmbH	Karlsruhe, Germany
HCl	Klinik farmacy	Munich, Germany
Tween-20	Carl Roth GmbH	Karlsruhe, Germany
Hämalaun	Apotheke des Klinikums RDI	Munich, Germany
Ethanol 100%	Merck	Darmstadt, Germany
Ethanol 90%	Merck	Darmstadt, Germany
Ethanol 50%	Merck	Darmstadt, Germany
Roticlear	Carl Roth GmbH	Karlsruhe, Germany
NaCl	Carl Roth GmbH	Karlsruhe, Germany
PBS	PAA Laboratories GmbH	
BSA (Albumin Fraktion V) proteasefrei	Carl Roth GmbH	Karlsruhe, Germany
DAPI	Sigma Aldrich	Missouri, U.S.A.
Hydrogenperoxide 30%	Carl Roth GmbH	Karlsruhe, Germany
Triton	Carl Roth GmbH	Karlsruhe, Germany

Devices and Software

Product	**Company**	**City, Country**
Computer	Dell	Frankfurt am Main, Germany
Vortexer	IKA Works INC.	Wimington, U.S.A.
Graph Pad	Graphpad Software Inc.	California, USA
ImageJ	National Institute of Health	Maryland, USA
Graphich Autodesk	Picta Inc.	California, USA
Keyence BioRevo BZ-9000	Keyence	Neu-Isenburg, Germany
Semi.sterile work bench	Hera guard, Thermo Science	Bonn, Germany

Primary antibodies

Product	Identification Number	Company	City, Country
Anti-αSMA	M0851, mouse monoclonal	DAKO	Hamburg, Germany
Anti-S100	MAB079-1, mouse monoclonal	Millipore	Massachusetts, U.S.A
Anti-CK19	sc6278, mouse monoclonal	Santa Cruz	Texas, U.S.A
Anti-CK19	sc25724, Rabbit polyclonal	Santa Cruz	Texas, U.S.A
Anti-CD31	ab-28364 rabbit polyclonal	Abcam	Cambridge, UK
Anti-CD45	DB042-1, rabbit clonal	DB Biotech	Kosice, Slovakia
Anti-CD8	Mob117, mouse monoclonal	Diagnostic Biosystems	California, U.S.A.
Anti-CD103	HPA036313, IgG rabbit	Sigma	Missouri, U.S.A.

Anti-FOXP3	ab20034, mouse monoclonal	Abcam	Cambridge, UK
Anti-CD4	HPA004252, rabbit polyclonal	Sigma Prestige	Missouri, U.S.A.
Anti-CD33	SAB4700737, mouse monoclonal	Sigma Aldrich	Missouri, U.S.A.
Anti-CD11	Ab52478, rabbit monoclonal	Abcam	Cambridge, UK
Anti-CD56	AB5032, rabbit polyclonal	Millipore	Massachusetts, U.S.A
Anti-Ki67	Ab15580, rabbit polyclonal	Abcam	Cambridge, UK
Anti-CD68	HPA048982, rabbit polyclonal	Sigma prestige	Missouri, U.S.A.
Anti-CD68	Mob167, mouse monoclonal	Diagnostic Biosystems	California, U.S.A.
Anti-HLA-DR	sc-56545, mouse monoclonal	Santa Cruz	Texas, U.S.A
Anti-CD206	HPA004114, rabbit polyclonal	Sigma Prestige	Missouri, U.S.A.
Anti-CD20	NCL-L-CD20-L26, mouse monoclonal	Leica	Wetzlar, Germany
Anti-mouse IG1	X0931 negative control mouse	DAKO	Hamburg, Germany
Anti-mouse IG2a	X0943 negative control mouse	DAKO	Hamburg, Germany
Anti-mouse IG2b	X0994 negative control mouse	DAKO	Hamburg, Germany
Anti-rabbit	X0903 negative control rabbit immunoglobuline fraction normal	DAKO	Hamburg, Germany

Secondary antibodies

Antibody	Specificity	Company	City, country
HRP anti-Mouse	Anti-mouse	DAKO	Hamburg, Germany
HRP anti-Rabbit	Anti-rabbit	DAKO	Hamburg, Germany
Alexa Fluor 488	Goat anti-mouse IgG	Thermo Fischer	Regensburg, Germany
Alexa Fluor 594	Goat anti-rabbit IgG	Thermo Fischer	Regensburg, Germany
Alexa Fluor 488	Donkey anti-goat IgG	Thermo Fischer	Regensburg, Germany

Selection of Patients

We designed a consecutive and retrospective observational case-serie study including 37 neoadjuvantly treated and 37 upfront resected matched patients diagnosed with PCa, who underwent surgical resection with curative intention between 2008 and 2015 at Klinikum Rechts der Isar of the Technical University of Munich.

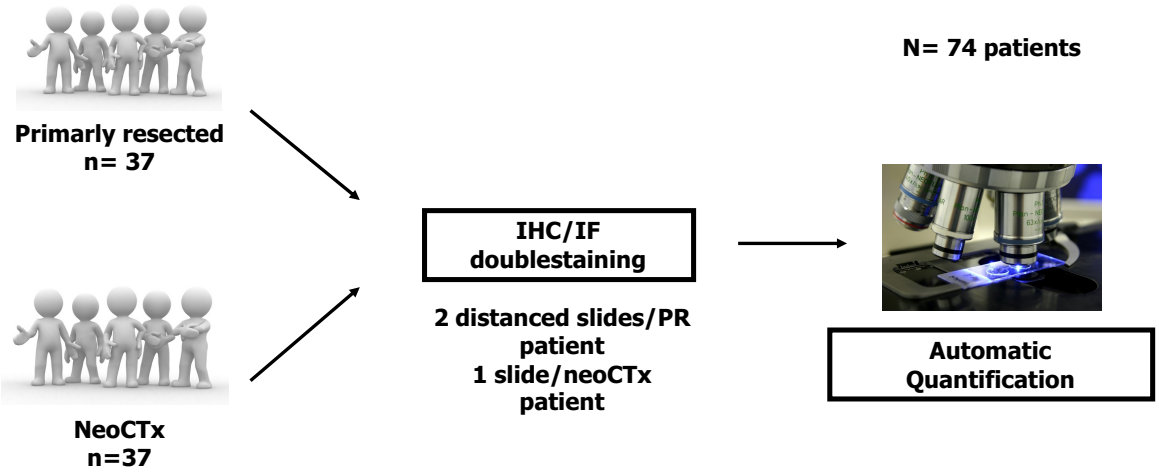

Figure 7. Schematic explanation of the study design

The applied neoTx regimens were of broad spectrum and included both chemotherapy and chemoradiotherapy regimens (Table 2). All the cases were conventional pancreatic ductal adenocarcinomas. Clinical and pathological data were obtained through a detailed retrospective review of the medical records of all 74 patients. The clinicopathological characteristics showed no significant difference in the two groups and are summarized in Table 3. All patients were informed, and written consent was obtained for tissue collection. The conservation and histopathological diagnosis were carried out by the Institute for Pathology at Klinikum Rechts der Isar. This study was approved by the Ethics Committees of the Technische Universtität München, Munich, Germany (Nr. 549/16s).

NeoCTx regime	**N° of patients (n=37)**
Gemcitabine mono	6 (16%)
Gemcitabine + Erlotinib	5 (14%)
Gemcitabine + Oxaliplatin	8 (22%)
Folfirinox	13 (34%)
Other regimes	5 (14%)

Table 2. Chemotherapeutical regimes

	Non-NeoTx (n=37)	**NeoTx (n=37)**	***p* value**
Sex			0.818
Male	21 (58.3%)	20 (54.1%)	

Female	16 (41.6%)	17 (45.9%)	
Age (year)	63.5 (46-82)	62.6 (47-78)	0.654
Tumor size (mm)	41.5 (3-90)	37.6 (15-100)	0.401
T Status			0.636
T1-T2	15 (41.6%)	20 (54.1%)	
T3-T4	21 (58.3%)	17 (45.9%)	
N Status			0.059
N0	11 (29.8%)	19 (51.4%)	
N1	26 (72.2%)	18 (48.6%)	
M Status			1.000
M0	31 (83.7%)	31 (83.7%)	
M1	6 (16.3%)	6 (16.3%)	
Grading			0.297
G1	2 (5.4%)	0 (0%)	
G2	18 (48.6%)	15 (45.4%)	
G3	17 (46.0%)	18 (54.6%)	
Resection Status			0.340
R0	18 (54.5%)	12 (38.8%)	
R1	14 (42.4%)	19 (61.2%)	
R2	1 (3.1%)	0 (0%)	
Tumor Localisation			1.000
Head	23 (62.2%)	26 (70.2%)	
Corpus	10 (27.0%)	5 (13.6%)	
Tail	2 (5.4%)	3 (8.1%)	
Head-corpus	1 (2.7%)	2 (5.4%)	
Corpus-Tail	1 (2.7%)	1 (2.7%)	
Surgical operation			0.634
Pancreatic head resection	21 (56.7%)	24 (64.9%)	
Distal pancreatectomy	11 (29.7%)	8 (21.6%)	
Total pancreatectomy	5 (13.5%)	5 (13.5%)	
Clinical manifestations			
Abdominal pain	13 (38.2%)	17 (65.4%)	0.038
Jaundice	15 (44.1%)	6 (23%)	0.093
Weight loss	9 (26.5%)	6 (23%)	0.768
New onset diabetes mellitus	3 (8.3%)	2 (5.4%)	0.626

Table 3. Clinical characteristics of neoadjuvantly treated vs upfront resected PCa patients

Immunhistochemistry (IHC) and immunofluorescence (IF)

For IHC, the sections were dewaxed in Roticlear® and rehydrated by washes in increasing grades of ethanol solutions. Antigens were retrieved by heating the tissue samples in citrate buffer/Tris Ethylenediaminetetraacetic acid (EDTA) buffer solution for 15 minutes. After rinsing in Tris-buffered saline, 0.1% Tween (TBST) (1x) solution, the sections were treated with Triton-X100 for 5 mins and rinsed again in TBST. Then, they were incubated in a 0.3% hydrogen peroxide solution for 10 minutes at room temperature to block endogenous peroxidase activity, rinsed in TBST buffer solutions

for 5 minutes and incubated with goat normal serum (GNS) or 3% bovine serum albumin (BSA) to block other antigen proteins. Next, we incubated the samples overnight in a Wet-box by 4°C with primary antibodies against αSMA, CD31 and CD56 at the concentrations specified in Table 2. Respective isotype control antibodies were used as negative control revealing no staining (anti-mouse IgG1, IgG2a, IgG2b and rabbit Ig normal fraction depending on the primary antibody species). After washing with TBST buffer saline solution (2 x 5 minutes), detection of primary antibodies was performed by using EnVision-HRP anti-mouse/anti-rabbit (respectively, if mouse or rabbit primary antibody were used) for 1h at room temperature. Diaminobenzene was used as the chromogen to visualize the samples and Haemalaun as the nuclear counterstain. After washing the sections under tap water for 15minutes, sections were dehydrated, cleared and mounted with Vecta Mount permanent mounting medium and Menzel-Gläser cover slips (24x40mm). Respective isotype control antibodies were used as negative control revealing no staining.

Buffer	Preparation
TBS (tris-buffered saline) (10x)	24g Tris + 85g NaCl Add distilled water to reach 1L and correct pH to 7.4
TBST (1x)	100ml TBS (10x) + 900ml distilled water + 1ml Tween 20
PBS (phosphate buffer saline) (10x)	95.5g PBS + 1000ml distilled water
PBST (1x)	9.55g PBS + 1000ml distilled water + 1ml Tween 20
Citrate buffer (20x)	21g Citric acid + 400ml distilled water Correct ph to 6.0 and complete to 500ml with distilled water
Citrate buffer (1x)	50ml Citrate buffer (20x) + 450ml distilled water
BSA 3%	3g BSA + 100ml TBST
Tris buffer	1.21g Tris + 0.37g EDTA + 0.5ml Tween Add millipore water to reach 1L and correct the pH to 9.0

Table 4. Specifications of the buffer solutions used in our analysis

Stromal component	Antibody	Species	Antigen retrieval	Blockin serum	Dilution	Secondary antibody
Neurogenesis/ Neural invasion	Anti-S100	mouse	Citrate	NGS	1:200	Alexa Fluor 488
	Anti-CK19	rabbit			1:50	Alexa Fluor 594
Angiogenesis	Anti-CD31	rabbit			1:400	HRP anti-rabbit

Stromal activation	Anti-αSMA	mouse		3%BSA/TBST	1:2000	HRP anti-mouse
Proliferation rate	Anti-ki67	rabbit		NGS	1:200	Alexa Fluor 594
	Anti-CK19	mouse			1:50	Alexa Fluor 488

Table 5. Specifications and dilutions of the primary antibodies used in the analysis of the PCa stroma

For the IF double-stainings, the tissue sections were dewaxed in Roticlear® and rehydrated by washes in increasing grades of ethanol solutions. Antigens were retrieved by heating the tissue samples in citrate buffer for 15 mins. After rinsing in Phosphate-buffered saline, 0.1% Tween (PBST) solution, the sections were treated with Triton-X100 for 5 minutes, rinsed again in PBST and then incubated with horse normal serum to block other antigenic proteins. Then, we incubated the samples overnight in a Wet-box by 4°C with primary antibodies and DAPI as nuclear stain. We performed the following double stainings: S100/CK19, ki67/CK19, CD45/CD8, ITGAE/CD8, FOXP3/CD4, CD33/CD11, HLA-DR/CD68, MRC1/CD68, CD45/CD20 (all details are summarized in Table 6). After washing with PBST buffer saline solution (3x10mins), sections were mounted using fluorescence mounting medium and Menzel-Gläser cover slips (24x40mm). Respective isotype control antibodies were used as negative control revealing no staining. We performed the histopathological analysis in two different regions of each resection specimen.

Immune cell population	Antibody	Species	Antigen retrieval	Blocking serum	Dilution	Secondary antibody
Cytotoxic T-lymphocytes	Anti-CD8	mouse	Citrate	Normal horse serum	1:40	Alexa Fluor 488 Alexa Fluor 594
	Anti-CD45	rabbit			1:400	
B-lymphocytes	Anti-CD20	mouse			1:200	
	Anti-CD45	rabbit			1:400	
T-regulatory lymphocytes	Anti-FOXP3	mouse			1:100	
	Anti-CD4	rabbit			1:80	
M1 macrophages	Anti-HLA-DR	mouse			1:200	
	Anti-CD68	rabbit			1:200	
M2 macrophages	Anti-CD206	rabbit			1:200	
	Anti-CD68	mouse			1:200	
MDSCs	Anti-CD11	rabbit			1:100	
	Anti-CD33	mouse			1:100	

DCs	Anti-CD103	rabbit	1:20
	Anti-CD8	mouse	1:40
NK cells	Anti-CD56	rabbit	1:600

Table 6. Specifications and dilutions of the primary antibodies used in our immune cell analysis

Quantitative analysis

Desmoplastic reaction

Tissue samples from primarily resected and neoadjuvantly treated PCa patients were stained with an α-SMA antibody and with the collagen-specific aniline blue of the Masson trichrome staining without applying hematoxylin or Biebrich scarlet acid as counterstain. Slides were digitally and entirely scanned with an automated digital brightfield microscope (Keyence BioRevo BZ-9000, Neu-Isenburg, Germany) at high-resolution and 10x magnification. The digital images were then analyzed for the total surface area versus stained area using ImageJ (National Institute of Health, Maryland, U.S.A). Briefly, the “color threshold” tool enabled us to select the blue-stained and the brown-stained pixels in the image histograms presented in the HSB (Hue, Saturation, Brightness) color space (Figure 8). Once the optimal thresholding values were determined, they were kept constant throughout the analysis. We then created a black mask of blue-stained and the brown-stained pixels representing the quiescent and activated component of the stroma respectively and measured its area. We also determined the already established activated stromal index (ASI) (28). Color artifacts and blood vessels were excluded manually from the analysis by the author. This was performed by meticulously encircling staining artefacts or blood vessels and deleting them from the image before measurements. For all values of the primarly resected cohort, the final statistics were calculated after obtaining the mean of the two values from the two analyzed sections from each patient.

$$\text{Collagen density} = \frac{\text{Blue stained area (collagen area)}}{\text{total area (mm}^2\text{)}}$$

$$\alpha\text{SMA density} = \frac{\text{Brown stained area (}\alpha\text{SMA area)}}{\text{total area (mm}^2\text{)}}$$

$$\text{Activated stroma index} = \frac{\text{Collagen area}}{\alpha\text{SMA area}}$$

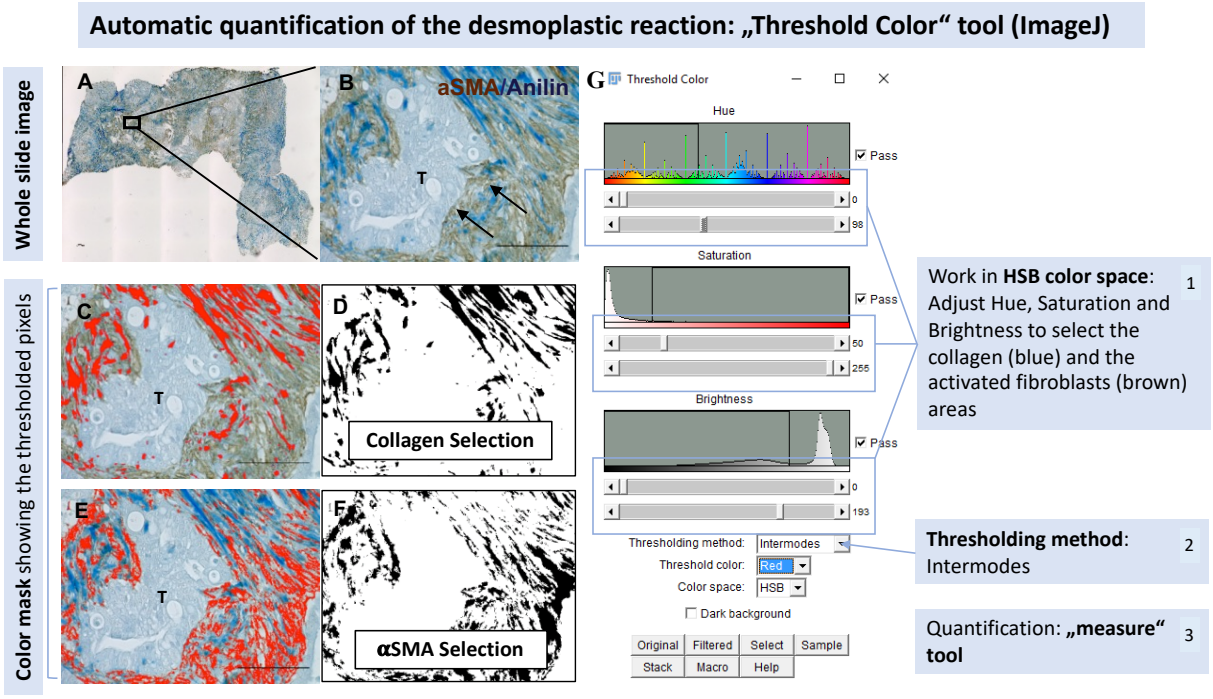

Figure 8. Schematic description of the automated quantification of the desmoplastic reaction using ImageJ Software. (A) Digitalized whole slide image scanned with Keyence Biorevo BZ-9000 microscope **(B)** Amplification of the selected region showing the αSMA specific staining of PSCs (black arrows) and the aniline blue-staining of collagen around a PCa tumor gland (T) **(C** and **E)** Overlay of the selected pixels in red over the original image. **(D and E)** Mask showing the selected areas for collagen and αSMA, respectively. **(G)** Interface of the “Threshold Color” tool in Image J

Angiogenesis

For the analysis of the angiogenesis, we calculated the proportion of endothelial cells stained with anti-CD31 using again an automated detection upon a preset threshold and the luminal area of the vessels selected manually on each sample (Figure 10), to the total area of the tissue. For this purpose, slides were entirely scanned with a digital brightfield microscope (Keyence BioRevo BZ-9000, Neu-Isenburg, Germany), at high-

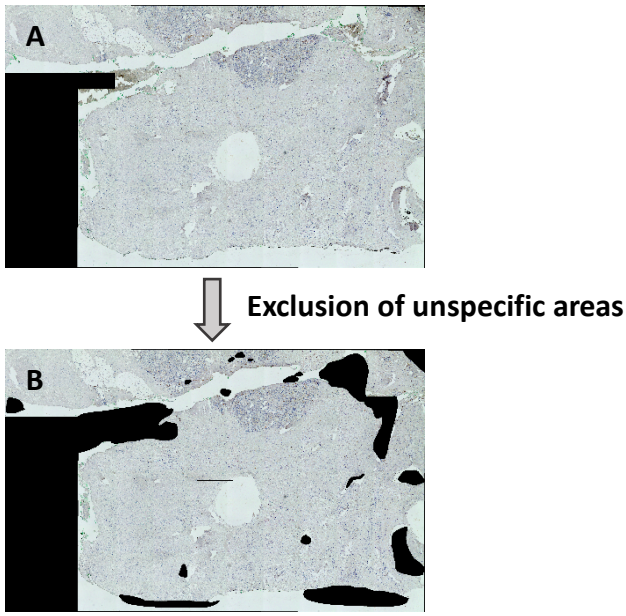

Figure 9. Exclusion of unspecific areas with the "free hand" and "clear" in ImageJ. A: Original merge image. **B:** Resulting image after clearing the unwanted areas

resolution and 10x magnification. ImageJ software was used for computerized quantification of immunostained vascular structures. DAB-positive pixels were selectively detected and uniformly displayed with red pixel overlay using the threshold function. Threshold parameters were defined by successively selecting regions on the Image histogram with intense DAB staining using the Hue-Saturation-Brighten 3D color space visualization and manually deleting regions of counterstaining and artefacts from the thresholded regions (Figure 9). These last two steps were repeated until all the DAB-positive pixels were selectively thresholded within the following thresholding limits: Hue 0-95, Saturation 10-165 and Brightness 0-255. Threshold settings were adjusted separately for each image (Figure 11). The thresholded immunostained area corresponding to endothelial cells was measured with the "Analyze Particles" command in ImageJ. We performed this analysis in the peritumoral niche defined as the circular area with a 150µm radius around the tumor cells, as well as on the whole tissue area.

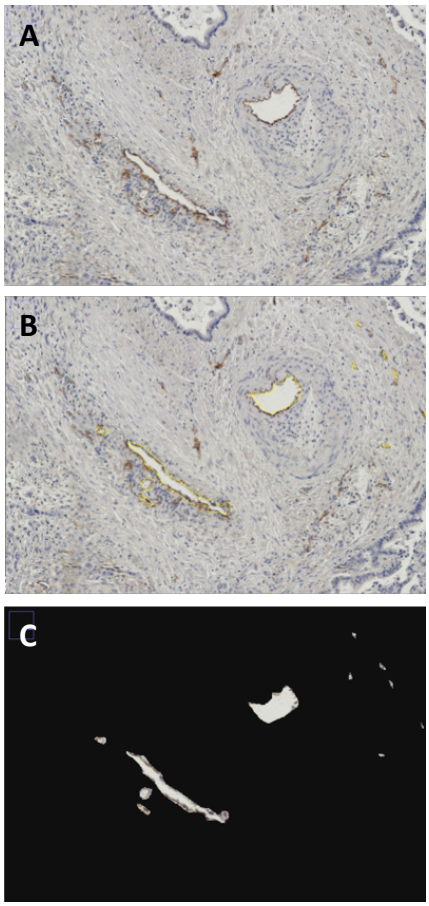

Figure 10. Selection of the microvessel lumen. A: Original merge image. **B:** Selection of the microvessel lumen using "free hand" tool in ImageJ. **C:** Measuring of the selected area

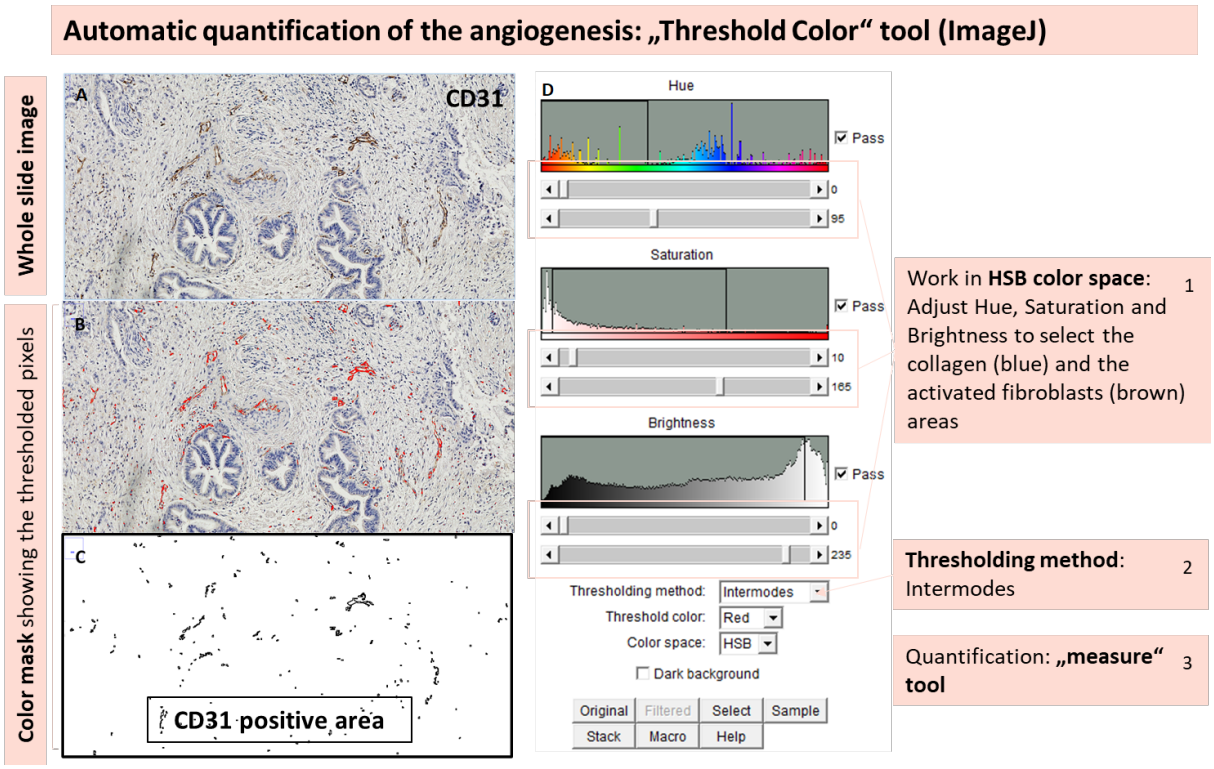

Figure 11. Schematic description of the automated quantification of the angiogeneis using ImageJ Software. (A) Brightfield image of CD31-staining showing the CD31 specific staining of endothel cells (brown pixels) (B) Overlay and (C) black mask showing the selected anilin-stained region. (D) Interface of the “Threshold Color” tool in ImageJ software.

The endothelial area was expressed as a ratio of the area (µm) of DAB-positive thresholded pixels compared to the total area of the image. The microvessel lumen area (MLA) was manually and meticulously selected with the free-hand tool of ImageJ and its area measured in each section (Figure 10).

$$\text{Endothel area} = \frac{\text{Surface of immunostained endothelial structure} * 100}{\text{total area (µm2)}}$$

$$\text{MA} = \frac{(\text{EA} + \text{microvessel lumen area}) * 100}{\text{total area (µm2)}}$$

All measurements were conducted in the whole tissue section and in the peritumoral area which was delineated by selecting tumor areas using the “free hand” tool and expanding this region 150 µm using the “expand” function in ImageJ.

Neurogenesis and NI

To determine the neural size, neural density and NI in our PCa human specimens, we performed an immunofluorescence double-staining using the glial marker S100 to detect the nerves and the epithelial marker CK19 to detect tumor cells present in the tissue samples. Using our digital epifluorescence microscope (Keyence BioRevo BZ-9000, Neu-Isenburg, Germany), we entirely scanned the sections at high resolution and 20x magnification. For its automated quantification, we used the "Hybrid cell count" algorithm of the Keyence Analyzer Software. First, the S100-immunostained area, corresponding to the nerves, was identified as "target area". Within the thresholding limits 15-25, the target area was then manually adjusted by the author, in order to remove unspecific staining. In the next step, we extracted the CK19-immunostained area within our already selected S100 positive area, setting again the thresholding limits between the values of 10 and 25 and manually deleting the unspecific areas not corresponding to tumor cells. If a CK19-positive signal was detected within a nerve, it was registered as endoneural invasion (ENI). Afterwards, we 5-fold expanded the target area and ran the extraction area algorithm to detect a possible CK19-positive signal around the immediate vicinity of the nerve, which was registered as perineural invasion (PNI). Nerves that presented with ENI were excluded from the detection of PNI (Figure 12). We defined following indexes to fully characterize PCa NI in our cohorts:

$$\text{PNI Index} = \frac{\text{N° of nerves with perineural invasion (PNI)}}{\text{total N° of nerves}}$$

$$\text{ENI Index} = \frac{\text{N° of nerves with endoneural invasion (ENI)}}{\text{total N° of nerves}}$$

$$\text{NI Index} = \frac{2\text{x}(\text{N° of nerves with ENI}) + \text{N° of nerves with PNI}}{\text{total N° of nerves}}$$

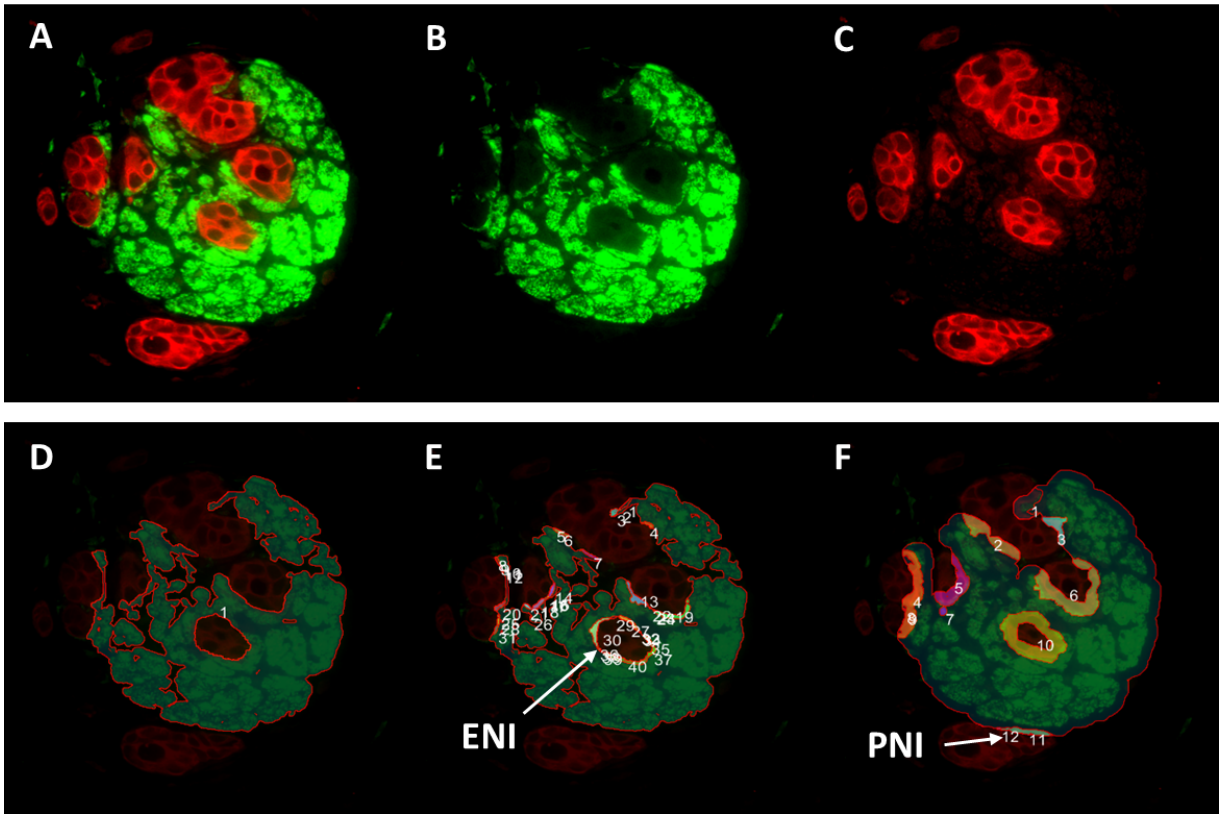

Figure 12. Automated analysis of pancreatic neuropathy in human PCa. (A) Representative images of an intrapancreatic nerve (green) invaded by tumor cells (white arrows). **(B)** S-100 specific immunostained area corresponding to the nerve (green). **(C)** CK19-immunostained pancreatic tumor cells (red) **(D)** Selection of the target area using the "Hybrid cell count" algorithm of the Keyence Analyzer Software corresponding to the S100-stained region. **(E)** Extraction of the CK19-stained area within the target area representing ENI. **(F)** 5-fold expansion of the target area and extraction of the CK19-positive regions. Please note the new detection of the presence of tumor cells in the immediate vicinity of the nerve, which corresponds to PNI.

Furthermore, we also characterized others features of PCa neuropathy. To determine the amount of neurogenesis, we used the neural density and neural area, whereas the hypertrophy of the nerves was measured using the medium nerve size. For all analyzed features, the final statistics were calculated after obtaining the mean of the two values from the two analyzed sections from each patient.

$$\text{Neural density} = \frac{\text{N° of nerves}}{\text{total area (µm2)}}$$

$$\text{Neural area (\%)} = \frac{\text{Area of nerves (µm2)} * 100}{\text{total area (µm2)}}$$

$$\text{Medium nerve size} = \frac{\text{Area of nerves (µm2)}}{\text{total N° of nerves}}$$

Tumor proliferation rate

In order to determine the proliferation rate of tumor cells after neoTx, we calculated the proportion of ki67$^+$ proliferating nuclei to both the absolute number of DAPI$^+$ tumor cell nuclei and to the tumor area using an automated detection upon a threshold after manually selecting the tumor areas on the tissue. For this purpose, slides were scanned with an automated digital brightfield microscope (Keyence BioRevo BZ-9000, Neu-Isenburg, Germany), at high-resolution and 20x magnification. Using the "free hand" tool of ImageJ, we were able to manually select the tumor areas and clear the tissue outside, which we considered background. We then separated the original composite image into its component channels using the "split channel" function on ImageJ. We then selected the DAPI$^+$ and ki67$^+$ nuclei using the "Threshold" tool on the respective 8-bit images and converted these images into masks representing the total nuclei of the tumoral area and the proliferating nuclei, respectively. As the nuclei often overlapped with one another, we performed a watershed segmentation before counting the thresholded objects with the "analyze particles" tool of ImageJ (Figure 13). The tumor proliferation rate was expressed as the number of ki67$^+$ proliferating nuclei compared to the total area of the image, whereas the tumor proliferation index was defined as the ratio of ki67$^+$ proliferating nuclei to the total number of nuclei in the tumoral area.

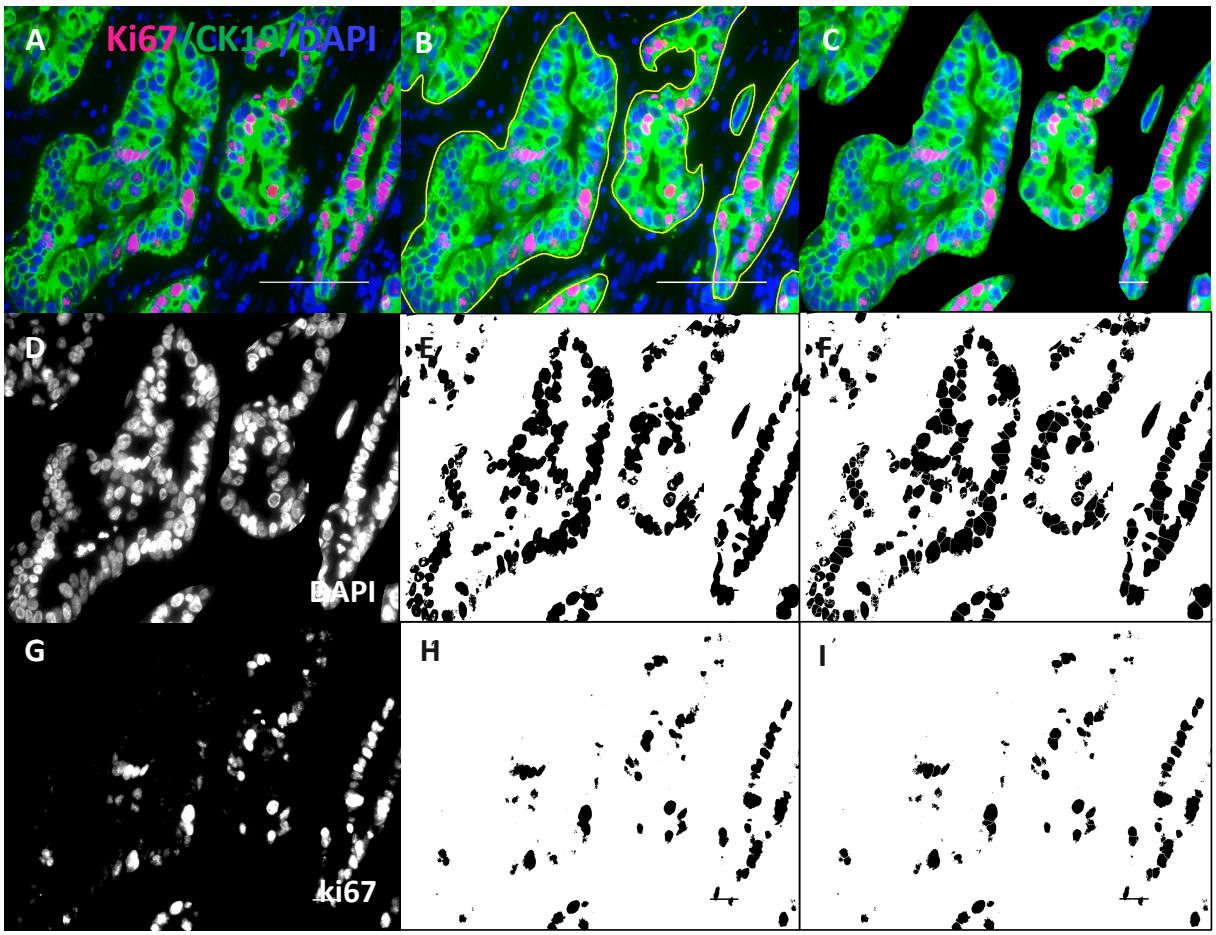

Figure 13. Software-based analysis of the tumor cell proliferation rate. **(A)** Original image. Please note that proliferating nuclei are stained with ki67 and present a pink color. **(B)** Manual selection of tumor area (green) using the „free hand" tool of ImageJ and measurement of this area. **(C)** Using the function "clear outside", we deleted the background (non-tumoral areas). **(D-E)** After splitting the composite image into its original channels, we were able to automatically detect all the nuclei present in the tumor glands by thresholding the $DAPI^+$ pixels **(F)** To assure the correctness of the analysis, before the automated quantification of the thresholded objects, we performed a watershed segmentation before counting the nuclei. **(G-H)** We then selected the ki67+ nuclei, representing the proliferating nuclei, using again the threshold function of ImageJ. **(I)** After performing a watershed segmentation, we counted the objects.

Immune cell analysis

The different lymphoid and myeloid immune cell populations were detected using double immunofluorescence labelling with the antibodies specified in Table 6. In order to specifically determine the immune cell infiltration in the tumor bed, a pre-analytical identification of the tumor bed was performed on consecutive H/E slides by Dr. med. A. Muckenhuber from the Institute for Pathology at Klinikum rechts der Isar, TUM. We transferred the marked area to our immunofluorescence-stained slides and using our Keyence microscope, we searched in tumor bed, regions highly infiltrated by immune

cells. High-resolution images were taken from each one of these areas. In every patient, we selected the 8 hotspots with the highest density of immune cells for further co-localization analysis. Each staining constituted a double immunostaining, where the aimed cell population was labelled with both specific antibodies. In order to detect these cells, we developed an experimental pipeline based on object-based co-localization using Cell-profiler pre-design modules. Here, we were able to detect if the cell membrane of immune cells presented one, two or none of the antibodies used and then assigned them to the corresponding immune cell population using a "relate-objects" algorithm (Figure 14).

- **Module 1**: Color-to-gray. We separated our composite image into its three channels (8-bit images)
- **Module 2 and 3:** Correct-Illumination-Calculate + Correct-Illumination-Apply. We calculated an illumination function and applied a median filter to smooth the images
- **Module 4:** Save-Images. We saved our images in our clipboard to be able to work on them later
- **Module 5.** Align. Since accurate co-localization requires accurate positioning of the objects in both images, we used this module to correct shifts in the optical path of the microscope in each channel of a multi-channel set of images.
- **Module 6:** Identify-Primary-Objects. It identifies components of interest in grayscale images containing bright objects on a dark background. To specifically select cells of interest, we used a global automatically-calculated threshold strategy and the Otsu Two-class thresholding method, which adapts to light changes in lighting/staining condition between images and is more accurate than manual thresholding strategies.

- **Module 7:** Relate-Objects: This module assigns relationships between cells. All objects within a parent-object become its children. If an object is touching multiple parents, the object will be assigned to the parent with maximal overlap.
    - Parent objects:
        - $CD45^+$ cells: for the cytotoxic T cell and B cell immunostainings
        - $CD68^+$ cells: for the M1 and M2 macrophage stainings
        - $CD11^+$ cells: for the MDSCs staining
        - $CD4^+$ cells: for the Treg cells staining
    - Child object:
        - $CD8^+$ cells: for the cytotoxic T cell staining
        - $CD20^+$ cells: for the B cell staining
        - HLA-DR^+ cells: for the M1 macrophages staining
        - $CD206^+$ cells: for the M2 macrophages staining
        - $CD33^+$ staining: for the MDSCs staining
        - $FOXP3^+$ staining for the Treg cells staining
- **Module 8:** Filter-Objects: it eliminated objects based on their parent-children relationship and removed all objects that do not pass a criterion. In this case, only those i.e. $CD8^+$ objects that fall into the co-localized children are retained.
- **Module 9:** Export-To-Spreadsheet. This module is used to export the full set of measurements obtained by the pipeline

For all analyzed features, the final statistics were calculated after obtaining the mean of the two values from the two analyzed sections from each patient.

1 Color-To-Gray

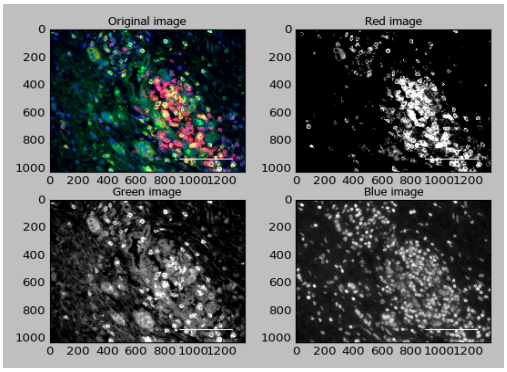

2 Correct-Illumination and Align

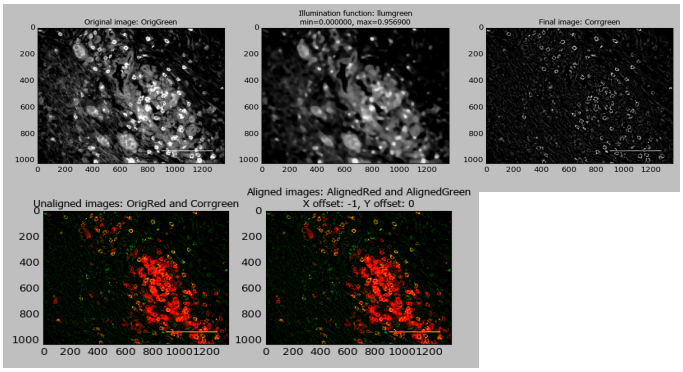

3 $CD8^+$ cells — Identify Primary Objects — $CD45^+$ cells

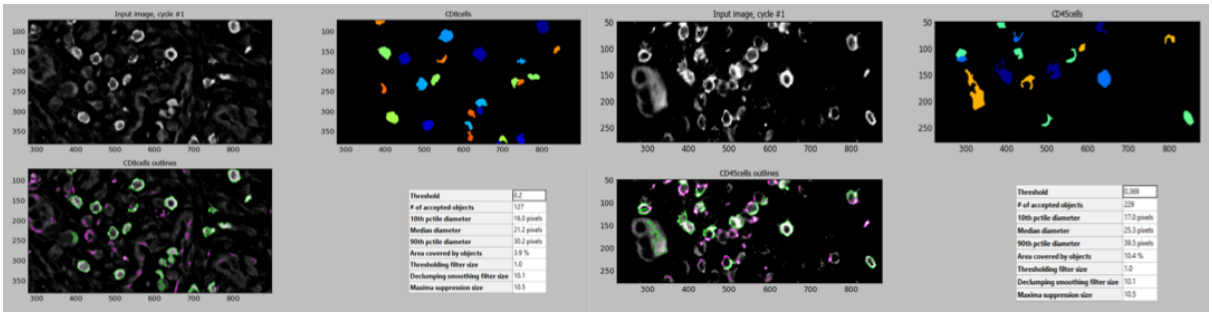

4 Relate Objects

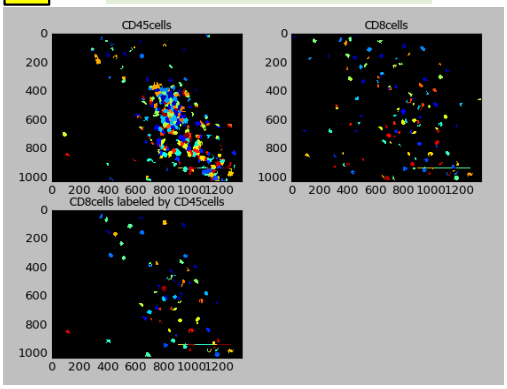

5 Filter Objects

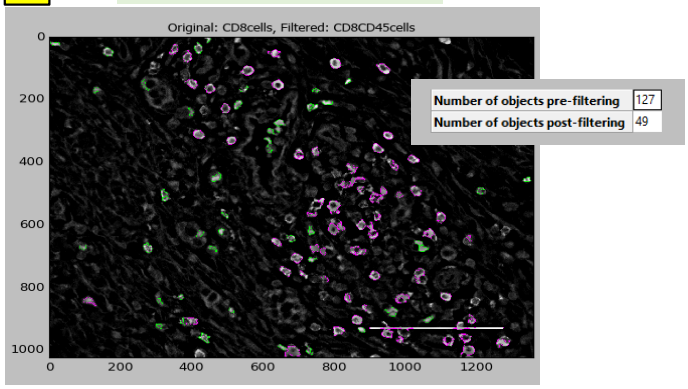

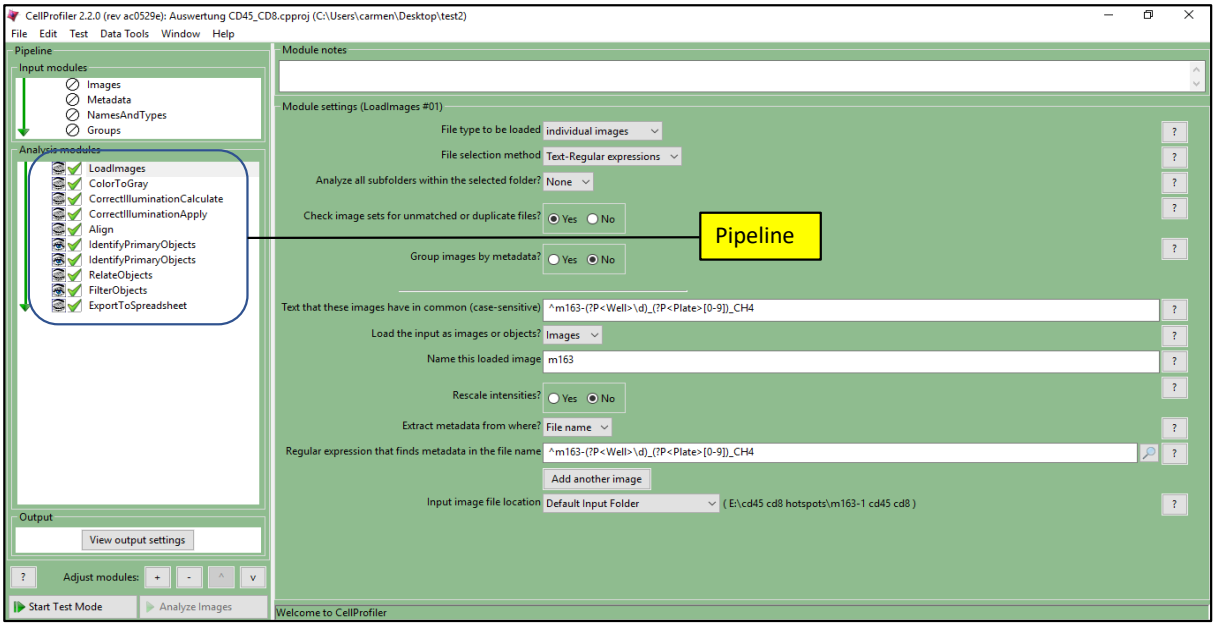

Figure 14. Detailed Cell-profiler pipeline used in the analysis of immune cell infiltration in the PCa microenvironment

Statistical analysis

Statistical analysis was performed using the IBM SPSS Statistics v25 (New York, U.S.A.) and GraphPad Prism 5 software (San Diego, U.S.A.) was used to design the graphics. The unpaired t-test was applied for two-group analysis. Multiple test correction was performed using the bootstrapping method in SPSS Statistics v25. Results are expressed as mean ± standard deviation (SD). Overall patient survival was calculated from the date of therapy start to the date of last follow-up (censored) or date of patient death (event). Median values were taken as cut-off limits in the comparison of 2 groups. Univariate survival analyses were calculated using the Kaplan-Meier method for estimation of event rates and the log-rank test for survival comparisons between patient groups. We used the Cox regression model to perform the multivariate analysis. The estimations of hazard ratios were presented with 95% confidence intervals. Comparison of demographic data was made using the chi-square test. To examine the correlation between immune cell subtypes and other members of the stroma, we used the Pearson´s coefficient. Two-sided p-values were always computed, and an effect was considered statistically significant at a p-value ≤ 0.05.

Results:

The tumor microenvironment of PCa after neoTx is characterized by reduced activation of the stroma and diminished NI

A strong desmoplastic reaction is a pathognomonic feature of PCa, and its role on tumor promotion and chemoresistance has been widely reported in the literature (69). We aimed to determine whether neoTx is able to alter the activity of PSCs and remodel the collagen deposition and stromal activation in the PCa microenvironment. Here, both the density of the PSCs activation marker αSMA (0.07514 ± 0.03273 vs 0.02094

± 0.01692; p=0.734) and the amount of "quiescent" stroma, characterized by the already deposited collagen, remained constant after neoTx (0.1593 ± 0.1741 vs 0.2763 ± 0.3248; p=0.394). However, the ASI revealed a significant reduction in neoadjuvantly treated patients (0.8581 ± 0.7822 vs 0.1151 ± 0.1136; p=0.003) (Figure 15B). Activated PSCs have been proposed to impede lymphocyte infiltration (33). These findings were supported by our correlation analyses, as the ASI was negatively correlated with the numbers of $CD8^+$ T cells (r=-0.3279, p=0.0043) and DCs in the vicinity of the tumor (r=-0.2583, p=0.0263).

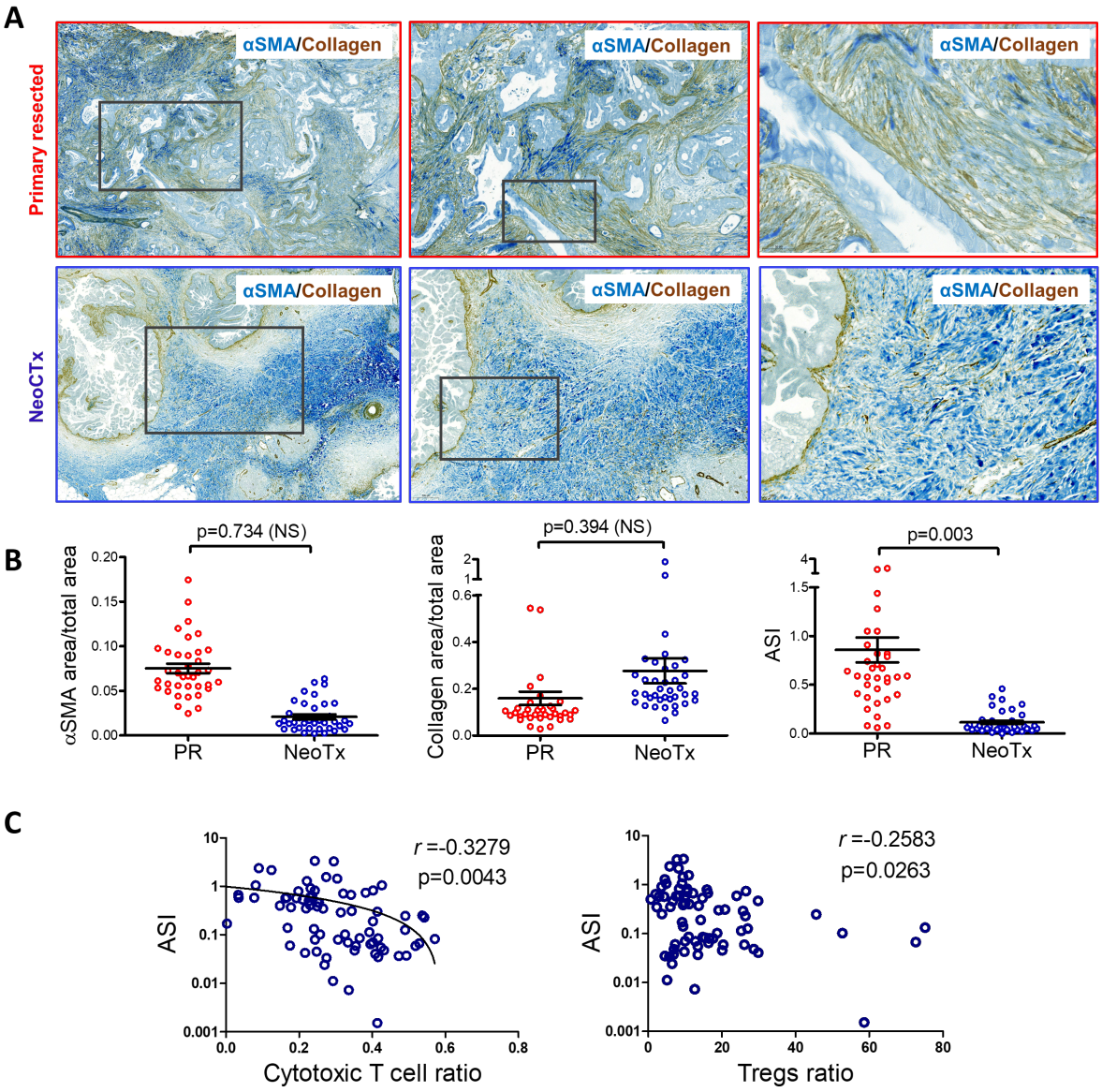

Figure 15. Histopathological effect of neoTx on the stromal activation of PCa. (A) Representative images of the immunohistochemical staining of αSMA and anillin, representing the activated and quiescent stroma,

respectively. Scale bars indicate 2000μm, 100 μm and 50 μm from the left to the right **(B)** Pairwise comparisons of collagen area, αSMA area and ASI on both neoadjuvantly treated and PR patients. **(C)** Correlation analysis between ASI and tumor-infiltrating immune cells.

Pancreatic neuropathy, including increased neural density and hypertrophy and the unavoidable presence of NI, is one of the hallmarks of human PCa. Neither the density of nerves (3.3 ± 2.3 vs 3.9 ± 2.5 nerves per mm^2; p=0.230) nor the neural size (15400 ± 36610 μm^2 vs 9772 ± 10550 μm^2; p=0.831) was modified by neoTx compared to upfront resected patients (Figure 16C). We observed, however, a 3-fold decrease in the severity of the NI by tumor cells (30.51 ± 21.75 vs 9.422 ± 12.70; p=0.001 on neoadjuvantly treated patients. On our separate analysis of the ENI and PNI, we obtained a notable decrease in both features after neoTx, which was more pronounced for PNI (12.39 ± 11.48 vs 4.064 ± 5.011, p=0.003; 18.37 ± 15.25 vs 5.214 ± 9.584, p=0.001, respectively) (Figure 16C). Furthermore, our results demonstrated a strong correlation between NI and the activation of the stroma (ASI) (r=0.3636, p=0.0014). The number of nerves present on the tumor microenvironment and the absolute area covered by neural cells, reflected by the neural density (r=0.1922, p=0.1009) and neural area (r=0.0734, p=0.5367), respectively, showed no correlation with the amount of activated PSCs (Figure 16B).

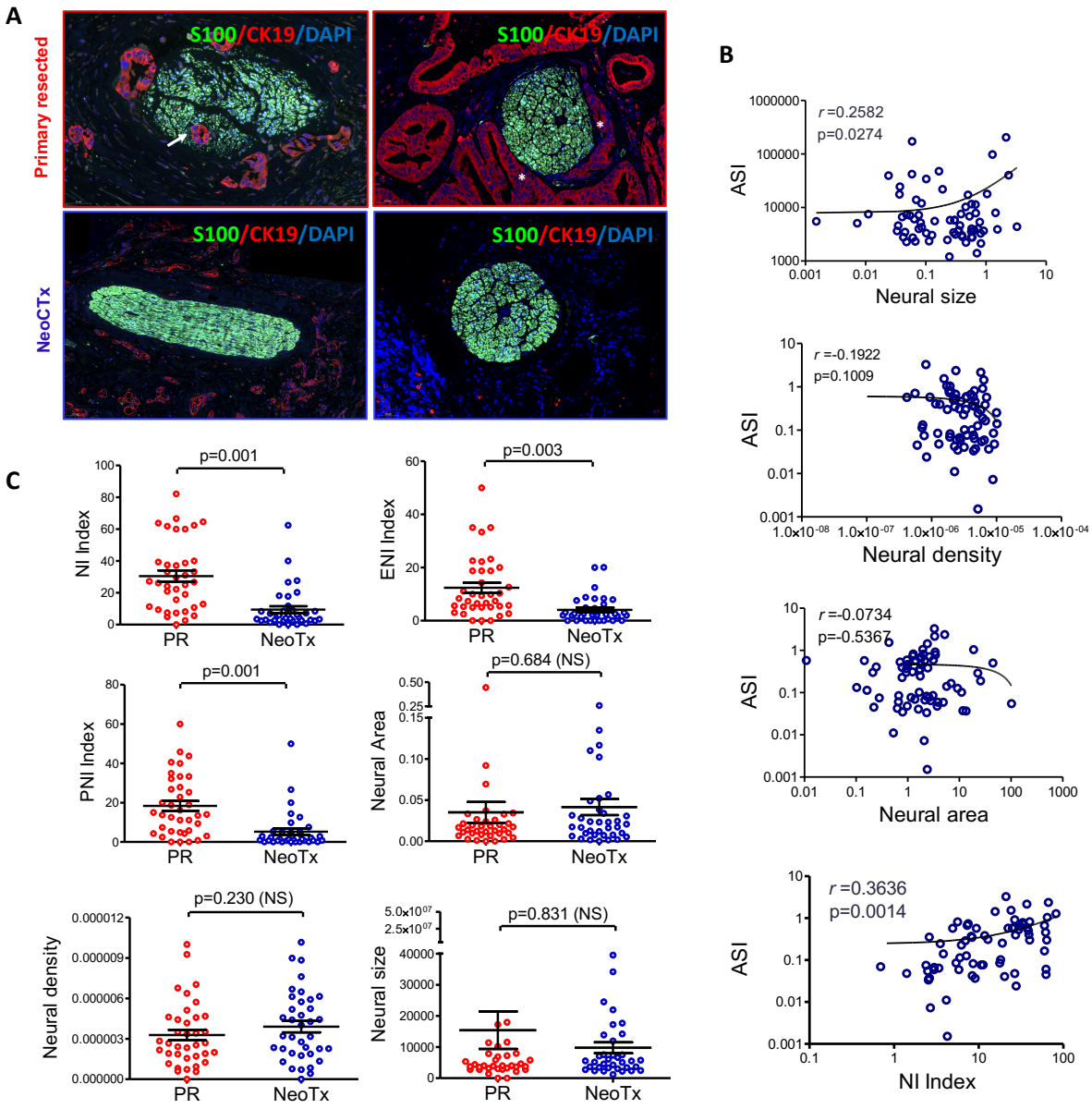

Figure 16. Histopathological impact of neoTx on NI in PCa (A) Representative photomicrographs of intrapancreatic nerves immunolabelled with the glial marker S100. Note that ENI (arrows) and PNI (asterisk) invasion are encountered more commonly in PR cases. Scale bars indicate 50 µm. (**B)** The neural size and NI show a positive correlation to the activation of the stroma, whereas the neural density and neural area are inversely correlated. Pearson correlation coefficient (r) and statistical significance are presented for both correlations. (**C**) Pairwise comparison of the severity of NI, ENI and PNI in neoadjuvantly treated patients vs PR cases demonstrate a decreased infiltration of nerves by tumor cells after neoTx. Neural density, area and size remain constant after neoTx.

The angiogenesis and proliferation rate of tumor cells in PCa microenvironment remain constant after neoTx

PCa is a scirrhous neoplasm, yet angiogenesis has been related to both tumor growth and immune cell trafficking. After neoTx, the absolute tumor vascularization remained constant, neither the endothelial area (EA) (0.002855 ± 0.001931 vs 0.002326 ± 0.001461µm^2; p=0.162) nor the microvessel lumen area (MLA) were altered after

neoTx (0.006258 ± 0.005861 vs 0.009823 ± 0.01289 μm^2; p=0.265). The analysis of the peritumoral area showed, likewise, no alteration of the angiogenesis in the vicinity of the tumor (peritumoral EA: 0.003096 ± 0.003895 vs 0.001821 ± 0.001438 μm^2, p=0.069; peritumoral MLA: 0.002866 ± 0.003498 vs 0.001721 ± 0.005213 μm^2, p=0.2729) (Figure 17A and B). In line with these results, the tumor proliferation rate proportioned to tumor area (0.0002033 ± 0.0001594 vs 0.0002000 ± 0.0002874, p=0.961) or to the total cell count (0.07383 ± 0.06005 vs 0.06491 ± 0.06338, p=0.633) remained constant after neoTx (Figure 17C and D).

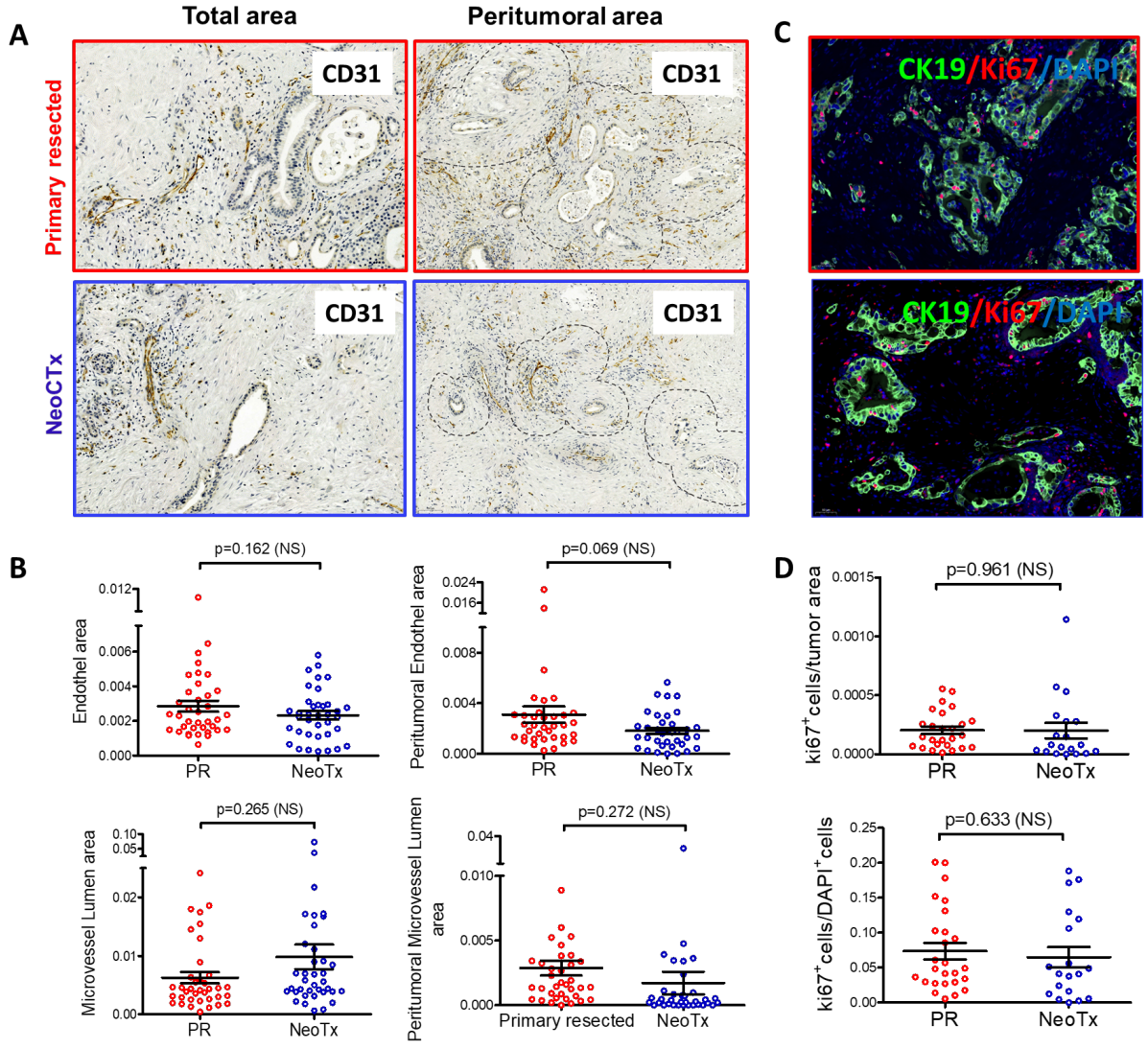

Figure 17. Histopathological effect of neoTx on the angiogenesis in PCa microenvironment. (A) Representative photomicrographs of CD31-stained areas representing the vascularization of the stroma (left, scale bars indicate 50 µm) and the respective analysis in the peritumoral area (right, scale bars indicate 100 µm) in

patients treated with neoTx vs upfront resected cases. The discontinuous line determines an area encircling a diameter of 150µm around tumor cells, defining the peritumoral niche. (**B)** Scatterplots showing the differences in endothelial area and microvessel density of the total and peritumoral area between primary resected and neoadjuvantly treated patients. **(C)** Representative images of CK19/ki67^{+}-stained tumor specimens representing the proliferating tumor cells (pink) among the CK19^{+} tumor cells (left, scale bars indicate 50 µm) (**D)** Scatterplots revealing no difference on the tumor proliferation rate between primary resected and neoadjuvantly treated patients.

However, we could demonstrate a strong correlation between the proportion of cytotoxic T cells and Tregs with the vascularity of the tumor (r=0.2471, p=0.0167 and r=-0.3009, p= 0.0092, respectively), which suggests a possible role of angiogenesis on immune cell trafficking, which is independent of neoTx (Figure 18A and B). The endothelial area, however, showed no association with intratumoral immune cells (r=-0104, p=0.9295 and r=0.2102 p=0.0723, for cytotoxic T cells and Tregs respectively) (Figure 18B and C).

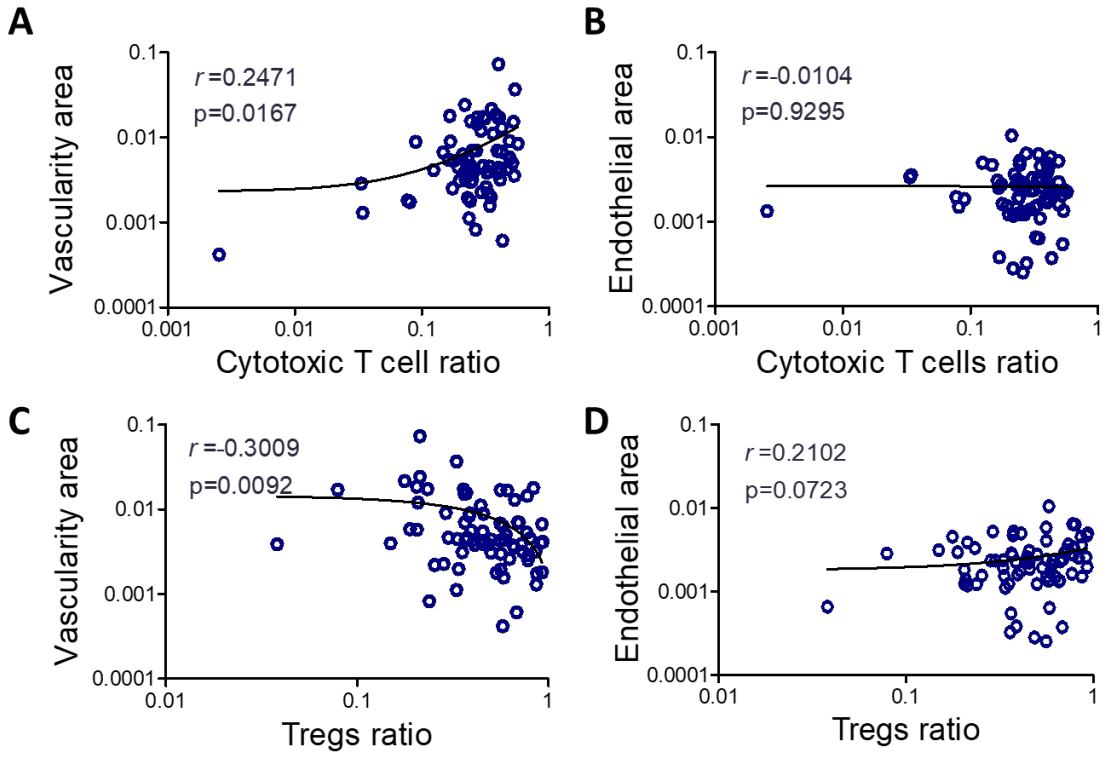

Figure 18. Correlation analysis between cytotoxic T cells (A, B) and Treg ratios (C, D) with angiogenesis

Proinflammatory and anti-tumor immune cell populations are significantly increased in the PCa microenvironment after neoTx

In order to determine the differences in the immune cell infiltration patterns between neoadjuvantly treated and primary resected tumors, we performed a comprehensive histopathological analysis of the immune response after neoTx in the juxtatumoral niche, including both proinflammatory and immunosuppressive immune cells. DCs are widely considered the most potent antigen-presenting cells in tumor immunity and our results demonstrated that after neoTx they doubled its initial density (10.07 ± 5.879 vs 21.72 ± 18.01cells/FOV, p=0.002) (Figure 19). We then analyzed the anti-tumorigenic $CD8^+$ T cell population. Although the density of $CD8^+$ infiltrating lymphocytes was similar in neoadjuvantly treated (56.20 ± 41.59 vs 64.43 ± 54.48cells/Field of view (FOV), p=0.425) and primary resected specimens, the proportion of $CD8^+$ T cells to the entire leucocyte population almost doubled after therapy (0.2265 ± 0.1139 vs 0.3713 ± 0.1019, p=0.001). The reason for this is that the total number of $CD45^+$ leucocytes was notably decreased in neoTx patients (267.7 ± 140.1 vs 188.7 ± 142.7 cells/FOV, p=0.027). Additionally, we demonstrated a positive correlation of $CD8^+$ lymphocytes with DCs (r=0.3301, p=0.0041) and M1 macrophages (r=0.3570, p=0.0018) (figure 20C).

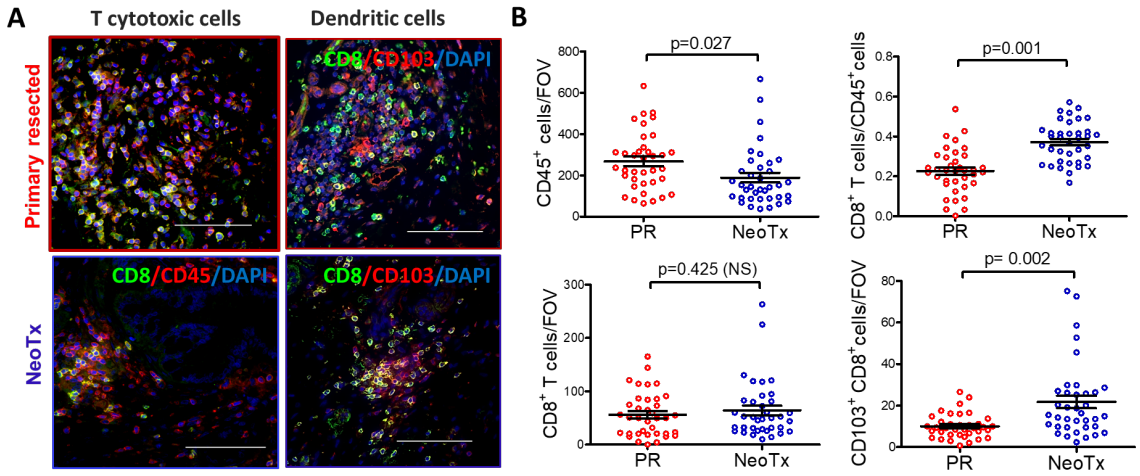

Figure 19. Histopathological impact of neoTx on anti-tumor immune cell populations (cytotoxic T cells and DCs) in human PCa (A) Representative photomicrographs (40x) showing the intratumoral infiltration by cytotoxic T-lymphocytes and DCs on primary resected (PR) vs neoTx PCa patients. **(B)** Scatterplot comparing the antitumorigenic immune cell infiltration, including $CD8^+$ cytotoxic T cells, $CD45^+$ cells and $CD8^+CD103^+$ DC between PR and neoadjuvantly treated patients. Each data point represents a single patient (median score of the 8 hotspots and lines represent the SEM). FOV: Field of view.

The density of NK cells, a cell subset of the innate immune response, classically considered to be able to recognize and destroy tumor cells, showed surprisingly a significant decrease (14.67 ± 12.24 vs 2.596 ± 2.654cells/FOV, p=0.002)and infiltrating CD8+ T cells were negatively correlated to the amount of NK cells (r= -0.4756, p=0.0001) (Figure 20B). The tumor infiltration by „classically-activated“ M1 macrophages, however, which have been reported to play an anti-tumorigenic role, remains unchanged after therapy (13.61 ± 9.968 vs 17.26 ± 10.71cells/FOV, p=0.155) and so did the entire CD68+ macrophage population (22.53 ± 15.03 vs 16.82 ± 12.28 cells/FOV, p=0.077). The proportion of HLA-DR+ M1 macrophages to the entire CD68+ macrophage population is slightly increased after neoTx (0.3100 ± 0.1564 vs 0.3884 ± 0.1561, p=0.034) (Figure 20B).

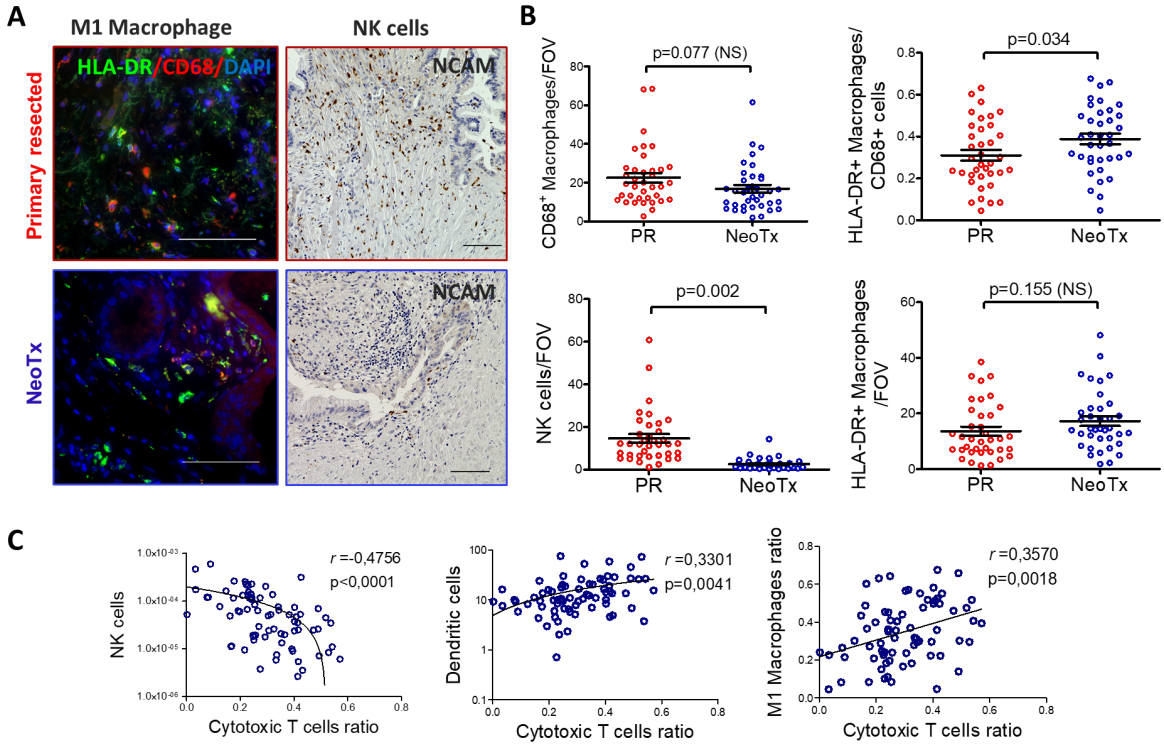

Figure 20. Histopathological impact of neoTx on anti-tumor immune cell populations (M1 macrophages and NK cells) in human PDA (A) Representative photomicrographs (40x) showing the intratumoral infiltration by M1 macrophages and NK cells on primary resected (PR) vs neoTx PCa patients. **(B)** Scatterplot comparing the antitumorigenic immune cell infiltration, including $CD68^+$ macrophages, $HLA\text{-}DR^+CD68^+$ M1 macrophages and $CD56^+$ NK cells between PR and neoadjuvantly treated patients. Each data point represents a single patient (median score of the 8 hotspots and lines represent the SEM). **(C)** Correlation analysis between the cytotoxic T cell ratio and the density of NK cells, DCs and M1 macrophages. FOV: Field of view.

The tumor infiltration by immunosuppressive cell subsets is significantly reduced after neoTx

Although the numbers of $CD4^+$ T cells remained constant (26.38 ± 13.95 vs 23.26 ± 14.20 cells/FOV , p=0.443), a subpopulation of highly immunosuppressive $FOXP3^+CD4^+$ Tregs underwent a significant reduction in both its density (15.04 ± 8.857 vs 10.21 ± 10.41 cells/FOV, p=0.057) and in its ratio to the whole $CD4^+$ T cell subpopulation (0.5792 ± 0.2272 vs 0.4200 ± 0.2011 , p=0.003) after neoTx. The intratumoral infiltration of MDSCs, a population of immature myeloid cells with the ability to suppress T cell activation (8) was also significantly reduced after neoTx (17.49 ± 15.05 vs 5.692 ± 5.460cells/FOV, p=0.002) (Figure 21B). Furthermore, the intratumoral infiltration of $CD8^+$ T cells was inversely correlated with the infiltrating $FOXP3^+$ Tregs (r=-0.3502, p=0.0022) (Figure 21C).

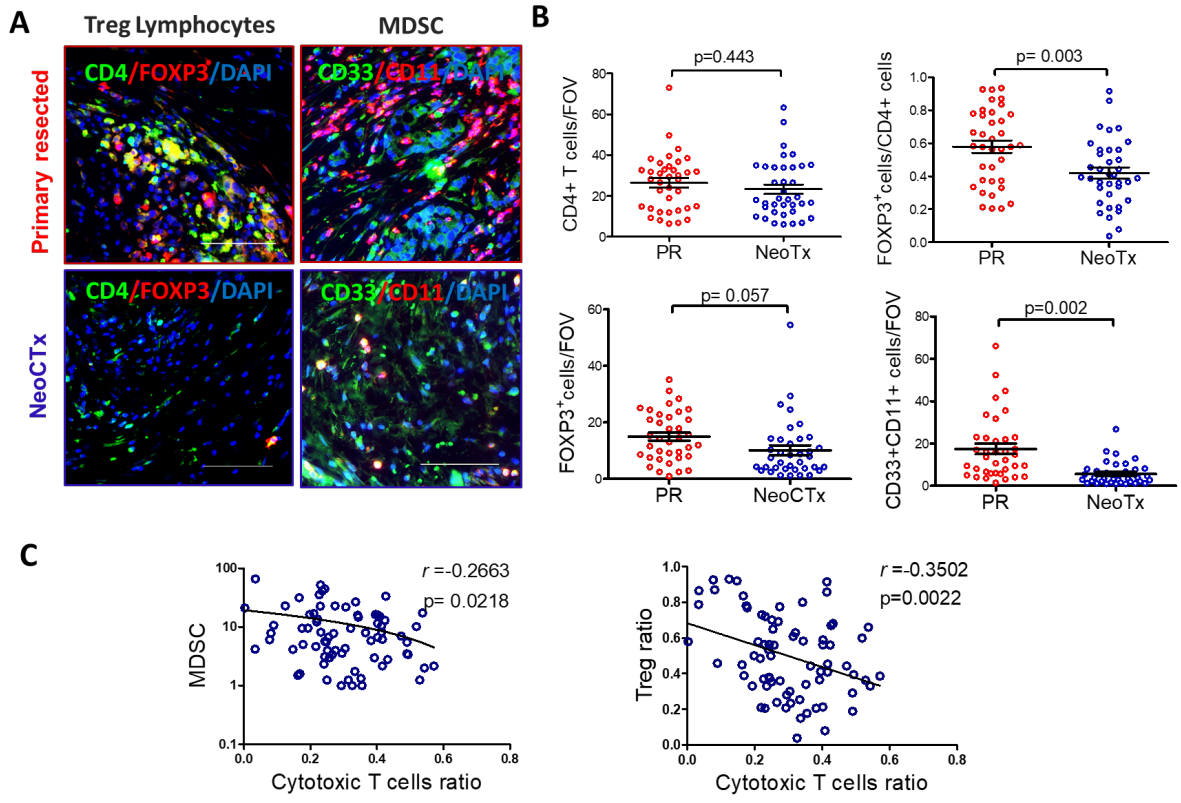

Figure 21. Histopathological impact of neoTx protumorigenic immune cell subsets (Tregs and MDSCs) in human PCa. (A) Representative photomicrographs (40x magnification) of immunolabelled Tregs and MDSCs of PR vs neoTx PCa patients. (**B)** Pairwise comparison of protumorigenic immune cell infiltration, including $FOXP3^+CD4^+$ Tregs, $CD4^+$ lymphocytes and $CD33^+CD11^+$ MDSCs between primary resected and neoadjuvantly treated patients. Each data point represents a single patient, median score of all hotspots (n=8) and lines represent the SEM. (**C**) Correlation analysis between the cytotoxic T cell ratio and the density of MDSCs and Tregs ratio.

Another lymphocytic cell subpopulation that has been reported to play a protumorigenic role in PCa are the $CD20^+$ B cells. Although not significant, we observed a decreased density of these cells (66.89 ± 63.17 vs 44.23 ± 58.57cells/FOV, p=0.079) as well as a reduction in their ratio to the entire leucocytic population in neoadjuvantly treated patients (0.1754 ± 0,1215 vs 0.1196 ± 0,1234, p=0.067) (Figure 22B).

Neither the absolute number of M2 macrophages (12.77 ± 12.42 vs 8.398 ± 6.659 cells/FOV, p=0.065) nor the proportion of M2 polarized macrophages (0.5215 ± 0.1783 vs 0.4530 ± 0.1637, p=0.065) to the total number of macrophages was altered after neoTx (Figure 22B). Additionally, we demonstrated a negative correlation of $CD8^+$ T cells to MDSCs (r=-0.2663, p=0.0218) (Figure 21C).

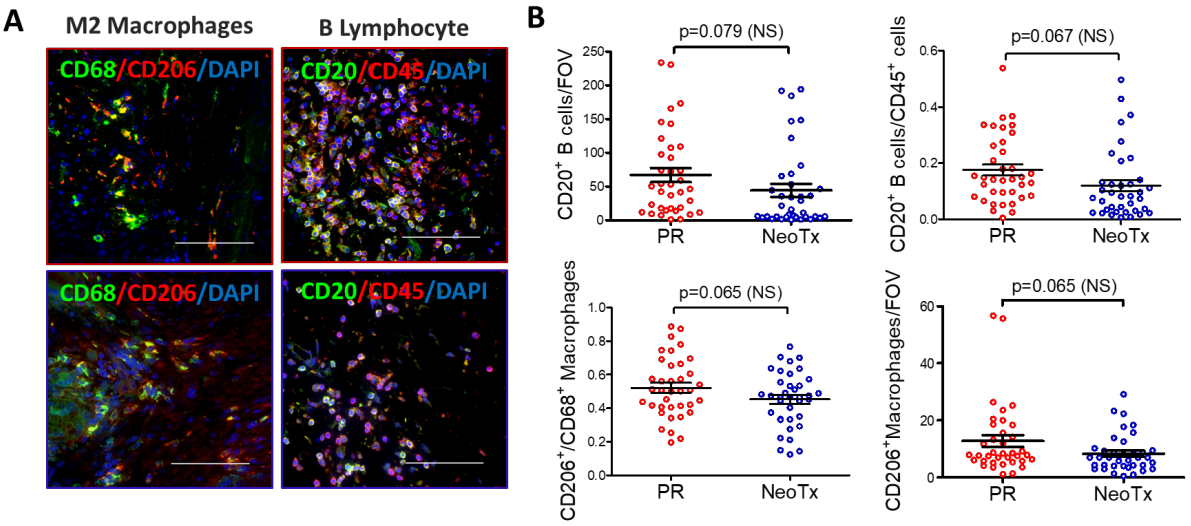

Figure 22. Histopathological impact of neoTx protumorigenic immune cell subsets (M2 macrophages and B lymphocytes) in human PCa. (A) Representative photomicrographs (40x magnification) of immunolabelled B-cells and M2 macrophages of PR vs neoTx PCa patients. **(B)** Pairwise comparison of protumorigenic immune cell infiltration, including $CD20^+CD45^+$ B-lymphocytes, $CD206^+CD68^+$ M2 macrophages and $CD68^+$ macrophages between primary resected and neoadjuvantly treated patients. Each data point represents a single patient, median score of all hotspots (n=8) and lines represent the SEM.

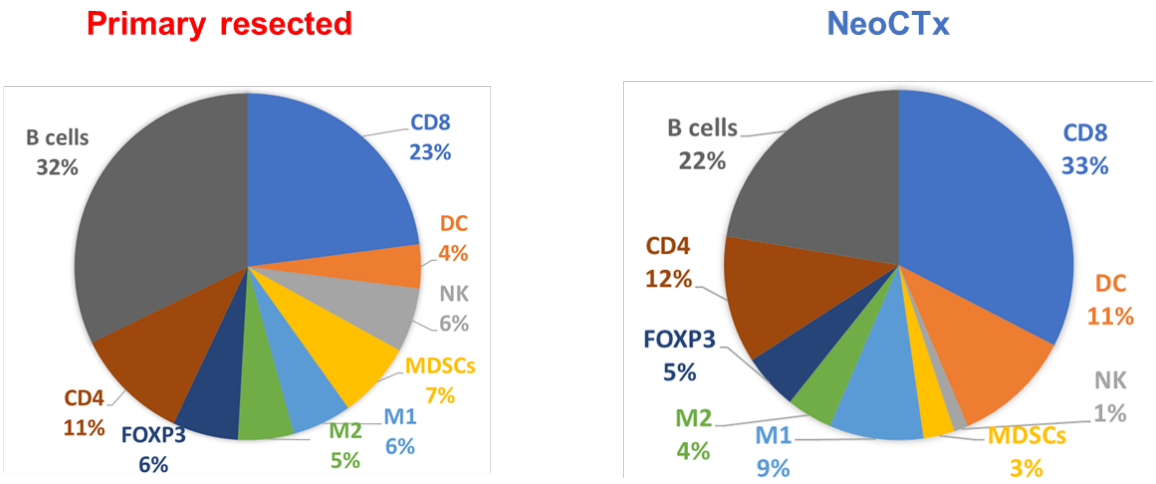

Figure 23. Relative distribution of tumor infiltrating immune cells in PR patients vs the neoTx group.

Clinical impact of the histopathological features of PCa microenvironment on survival

Although not significant, neoTx showed a beneficial effect on the clinical outcome of PCa patients with a median survival of 24 months from the day of therapy initiation against 14 months among primary resected patients (p=0.1181) (Figure 25A). We next performed an in-depth analysis of our histopathological and clinical data in order to identify possible predicting factors for survival for borderline resectable and locally advanced PCa. Median values of the cohorts were used as cut-offs except for NI and $CD4^+$ T cells, where preliminary analysis demonstrated that the use of percentile 75 and 25, respectively, was able to predict more accurately the progression of the tumor. In our univariate analysis, we showed that histopathological features such as ASI (p=0.0157), NI (p=0.0392) and the intratumoral infiltration with $CD4^+$ T cells (p=0.0475) and NK cells (p=0. 0514) were able to predict survival similarly to traditionally recognized prognostic factors like lymph node status (p=0. 0793), surgical margins (p=0.0232) and grade of differentiation (p=0. 0316) (Figure 24A-E and 25B-D)). Furthermore, patients with high tumor proliferation rate showed a much lower overall survival (14 months) than PCa with low proliferation rates (40 months) (p=0.0013).

Here, no patient with high proliferation rate presented with a long-term survival (Figure 24F). To assess the interdependence of these histopathological features, we performed a Cox regression analysis. Multivariate analysis revealed that, high vs low tumor proliferation rate (p=0.017), ASI (p=0.027), and high vs low infiltration of $CD4^+$ T cells (p=0.052) and NK cells (p=0.038) were independent prognostic factors in PCa, independent of the pre-treatment status (Table 4).

	Median survival (mo)	p value univariate	p value multivariate	Hazard ratio (95% CI)
Nodal status (N0/N1)	24.0/14.0	0.0793	0.001	0.618 (0.361-1.058)
Surgical margins (R0/R1-2)	24.0/14.5	0.0232	0.023	0.537 (0.314-0.918)
Differentiation (G1-2/G3)	28.0/14.0	0.0316	0.032	0.552 (0.322-0.949)
ASI	24.5/13.0	0.0157	0.027	0.488 (0.273-0.873)
NI index	24.0/13.0	0.0392	0.732	0.488 (0.247-0.965)
$CD4^+$ T cell density	16.0/23.0	0.0475	0.052	1.989 (1.008-3.927)
$CD56^+$ NK cells	24.0/13.5	0.0514	0.038	0.591 (0.340-1.025)

Table 7. Univariate and multivariate survival analysis for prognostic relevant clinical and histological features. Lymph node status, surgical margins and grade of differentiation were divided into negative and positive groups, while the infiltration with immune cells were divided into low and high groups using the median as cut-off value for ASI and NK cells, the 25 percentile for $CD4^+$ T cells and the 75 percentile for NI as they appeared to predict more accurately the tumoral behavior. We used the log-rank test for the univariate analysis and the calculation of the hazard ratio and a Cox regression for the multivariate analysis. CI: confidence interval

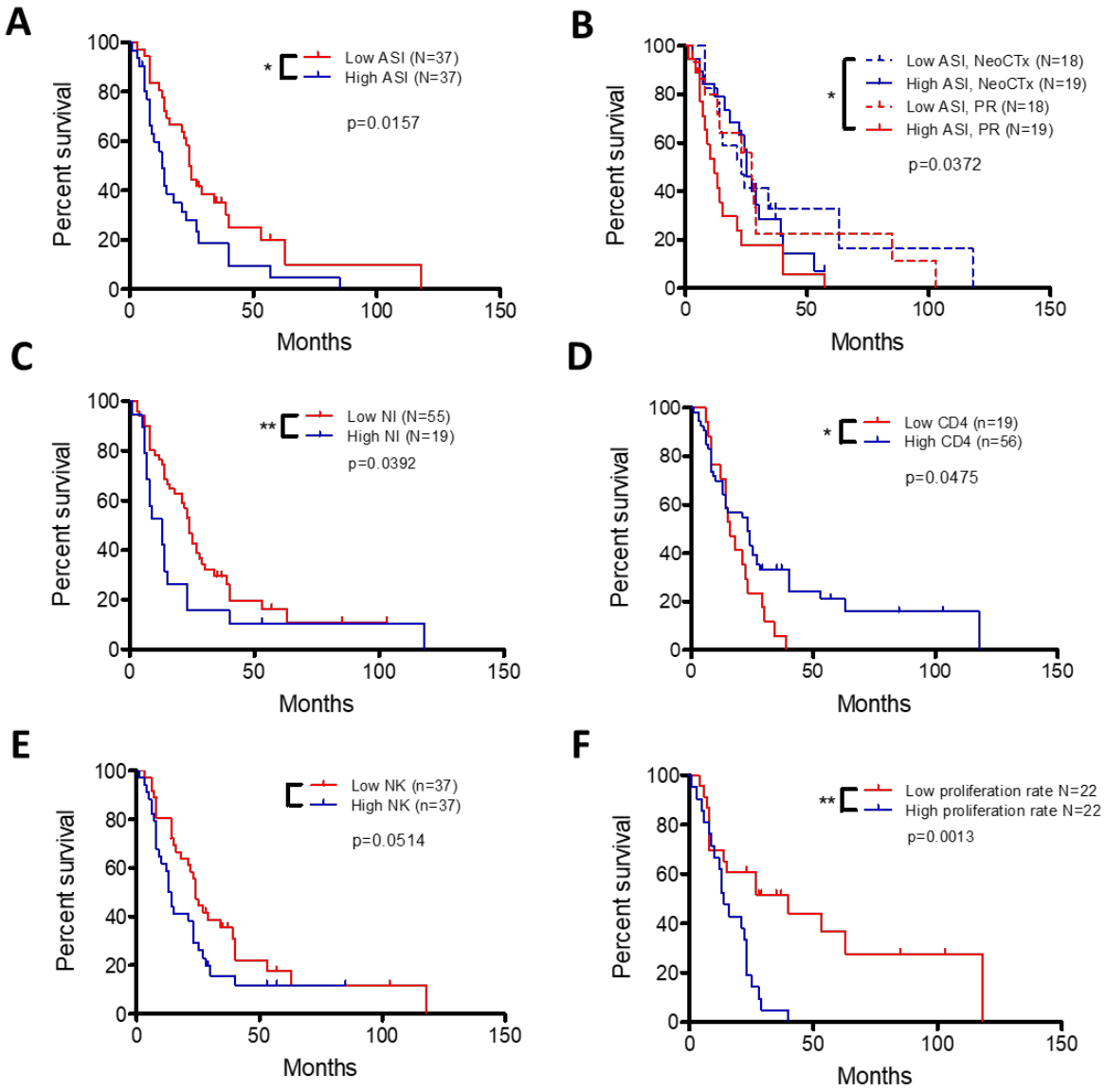

Figure 24. Survival analysis of all 74 PCa patients based on the histopathological features that have an impact on the clinical outcome of PCa patients. (A) Kaplan-Meier survival curves that show that the activation of the stroma (ASI) negatively correlates with survival. **(B)** The stratified analysis of ASI between neoadjuvantly treated and PR cases showed also statistical significance. NI **(C)**, together with the intratumoral infiltration of several immune cell types including CD4+ T cells **(D)** and NK cells **(E)** and the tumor proliferation rate **(G)** were correlated with the patients´ survival. High and low ASI and intratumoral infiltration values were divided based on the median value of the variables, except for NI where the 75-percentile was used. For the CD4+ cell density, the 25-percentile showed to predict survival more accurately than the mean. Significance was calculated using the log-rank test.

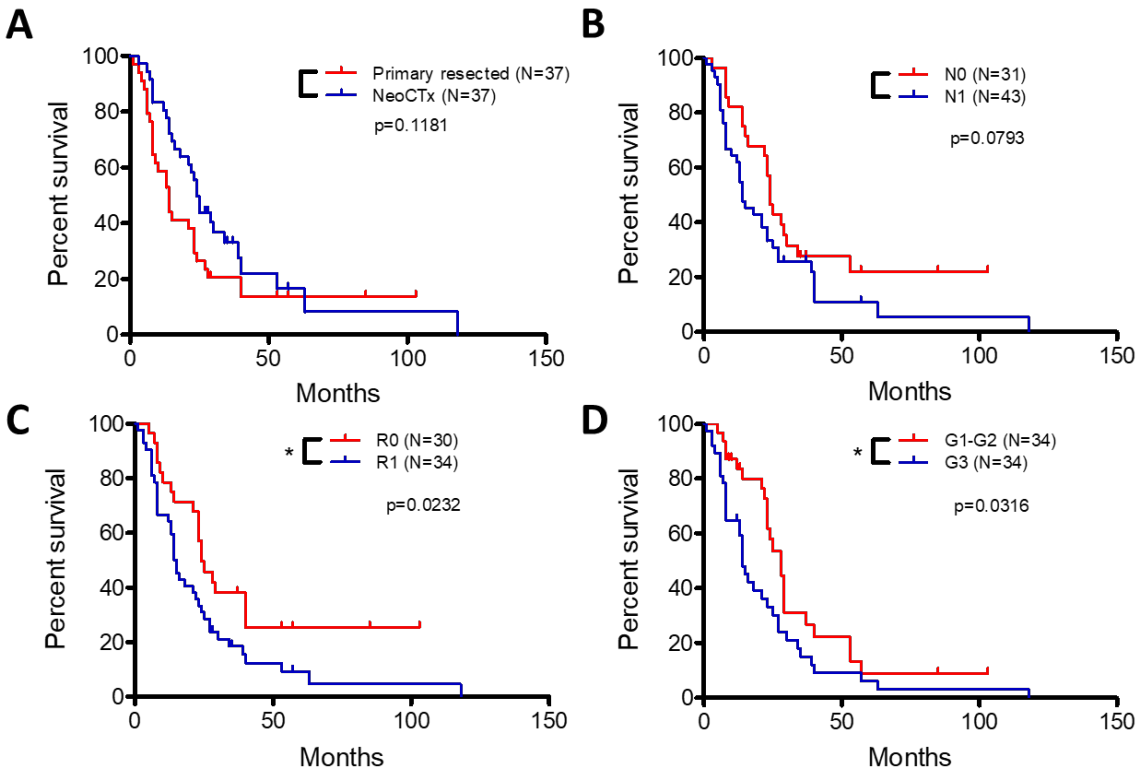

Figure 25. Survival analysis of PCa patients based on clinical features: application of neoTx **(A)**, lymph node status **(B)**, surgical margins **(C)** and the grade of differentiation **(D)** were found to influence patients´ overall survival. Significance was calculated using the Breslow-Wilcoxon test.

Discussion

Neoadjuvant therapies in borderline resectable and locally advanced PCa have led to a significant survival benefit over the past 10 years. With this study we demonstrated the ability of neoadjuvant approaches to suppress the protumorigenic immune cells, stromal reaction and NI. Increased infiltration by cytotoxic T cells, M1-polarized macrophages and DCs was predominant on the neoadjuvantly treated patients, whereas MDSCs, Tregs and NK cells, together with increased activation of PSCs and NI, dominated the PCa microenvironment of primarly resected PCa patients. These findings suggest that the beneficial effect of neoTx may not rely as traditionally believed on the direct cytotoxicity of chemotherapeutical agents but on a reactivation of the antitumoral immune response mediated by neoTx, which highlights the urgent need of new therapeutic strategies, especially neoadjuvant immunotherapy (20).

A strong desmoplastic reaction mediated by activated PSCs and the expression of stimulating cytokines has been associated with higher grade malignancies and poor prognosis in PCa (14, 28, 31). Our results confirmed the critical role of activated PSCs on the clinical outcome of patients, as the ASI constitutes an independent prognostic factor for PCa. Moreover, our findings suggest that the activation of PSCs is reversible after neoTx, and hence an important potential therapeutic target (70). In the past decade, however, the depletion of the stroma in the tumor microenvironment of PCa has led to more aggressive tumors with decreased survival (29, 69, 71). Recent research of the Tuveson group on PCa organoids and PSCs may have found an explanation for this inconsistency: they identified two subtypes of PSCs in the PCa microenvironment with potentially different pathophysiological functions. The periglandular $aSMA^{high}$ myofibroblastic fibroblast is likely to restrain tumor growth, whereas the diffusely distributed $aSMA^{low}$ $IL6^{+}$ inflammatory fibroblasts promote tumor growth by the expression of ECM and protumorigenic cytokines (72). According to our survival analysis where decreased ASI after neoTx correlates with increased survival, we could infer that neoTx possibly aims at the $aSMA^{low}$ $IL6^{+}$ inflammatory fibroblasts. Functional analyses, however, are urgently needed to elucidate the specific role of neoTx on the different subtypes of PSCs. Furthermore, PSCs account for immunomodulatory properties by preventing $CD8^{+}$ T cells from targeting PCa cells due to the secretion of CXCL12 chemokine (26, 27, 50). Our results confirmed an inverse correlation between the ratio of cytotoxic T cells and the activation of the stroma. PSCs have also been associated with the recruitment of MDSCs via expression of GM-CSF (73); our analysis showed, however, no correlation of the desmoplastic reaction and the infiltration with MDSCs. Tregs and NK cells were positively correlated with the ASI, and this feature has not yet been described in the literature and therefore requires further mechanistical experiments to elucidate the regulating mechanisms. All these

data point to a key immunoregulatory role of the stroma. Rendering activated PSCs quiescent through neoTx could improve, therefore, the access of proinflammatory immune cells into the juxtatumoral space.

The paucity of functional vasculature close to PCa tumor cells due to the high interstitial pressure in the tumor microenvironment is well established (32, 35). According to our results, the vessel density is not altered by neoadjuvant approaches. As previous studies stated, endothelial cells play an important role in immune cell trafficking and showed to be strongly correlated to the intratumoral infiltration of $CD8^+$ T cells and Tregs. However, this does not seem to be the principal mechanism of the immunological reactivation after neoTx as both the EA and the MLA remain constant after therapy. Interestingly, the numbers of $CD8^+$ T cells and Tregs were only related to the lumen of the blood vessels and not to the presence of endothelial cells, which also suggests that only non-collapsed vessels in the tumor microenvironment may play a functional role in the modulation of the immune cell infiltration.

The tumor-promoting effects of neuronal cells in PCa and the trophic support of cancer cells for nerves, result in complex neuroplastic alterations in the PCa microenvironment (74). Consistent with our data, Chaterjee et al showed that PNI was present in 80% of the upfront resected patients, which was significantly higher than 58% in the 212 neoadjuvantly treated patients (75). In our cohort, the severity of NI Index exhibited a 3-fold decrease after neoTx. The presence of severe NI has been related to strong desmoplastic reaction in PCa (76), which is also confirmed by our correlation analysis. PSCs have been proven to enhance the proliferation, migration and invasion of PCa tumor cells in a paracrine fashion (41, 77). The decreased number of activated PSCs observed after neoTx and reduced secretion of neurotrophic factors after neoTx, could partly explain the reduced NI present in neoadjuvantly treated patients. Contrary to

chronic pancreatitis and consistent with our results, PCa fibrosis seems to be independent of the number of nerves present in the tumor microenvironment (76), pronounced activation of the stroma correlated, however, with large hypertrophic nerves. NeoTx exerted no effect on the nerve density, size or innervation area, which suggest that the presence of numerous hypertrophic nerves is part of the early stages of PCa neuropathy and is irreversible by the time of chemotherapeutic administration. This was also proved by Stopczynski et al. who showed that in the KPC mouse model of PCa, increase in nerve density and augmented expression of neurotrophic factors in the pancreas occurs already during the PanIN stage (78). NI not only develops at a later stage, it appears to be triggered by a different molecular pathway in which activated PSCs play a key mediator role (40, 76). NeoTx is able to interfere with this crosstalk (Figure 3) and reverse the invasion of nerves by tumor cells, hampering an important way of cancer spread and tumor recurrence (79). Increasing evidence shows that the severity of the NI significantly impacts overall survival (76, 80). Accordant with the existing data, we showed a prolonged overall survival of patients with low NI, which again highlights the importance of the generation of NI-targeting therapies (75, 81).

The role of immune cells on tumor progression and their correlation with patients´ survival has been subject to investigation over the past decade. While the majority of the studies focus on the prognostic significance of isolated immune cell types, specially $CD8^+$ T cells (24, 51, 52), we adopted a wide-ranging approach in order to understand the interrelationship between the different members of the immune system and stromal components. It has been recently reported that several chemotherapeutical agents, not only exerted a direct cytotoxic effect on cancer cells, but also featured an alluring side effect by depleting immunosuppressive leucocyte subsets (8). In line with these reports, we observed that whilst PCa tissues present a significantly higher density of

cytotoxic lymphocytes, M1-polarized macrophages and DC after neoTx, the reverse was observed for MDSCs, Tregs and, paradoxically, for NK cells, with an equal density of B lymphocytes and M2 macrophages. These findings strongly suggest that the presence of an antitumoral immune response induced by neoTx could restrain tumor growth and cancer aggressiveness, urging further research on neoadjuvant immunotherapy (68).

The neoTx "timing" may be the key factor that could lead to successful immunotherapy on PCa. The efficacy of immunotherapy on PCs has been hampered by the low immunogenic potential compared to other solid malignancies like melanoma (82) and its predominantly immunosuppressive microenvironment dominated by Tregs and MDSCs infiltration (82, 83). We hypothesize that neoadjuvant regimes may unleash a more efficient and long-lasting antitumor immune response compared to adjuvant therapies mostly due to the presence of the tumor burden serving as antigen source for DCs-mediated priming and expansion of T cells (67, 84-86). Preclinical studies on experimental immunotherapies for advanced melanoma and PCa (anti-PD1, anti-PDL1, anti-CD137 and anti-CD25) have already demonstrated that the survival benefit is undoubtedly associated with the neoTx timing (87, 88), thus our study further emphasizes the immunological potential of neoTx on PCa.

The first study that analyzed the immunological impact of neoTx on PCa was carried out by Homma et al. and reported significantly higher numbers of $CD8^+$ and $CD4^+$ T cells and a reduction of the density of $FOXP3^+$ Tregs (67) after therapy. $CD8^+$ T cells constitute the most prevalent T cell population in human PCa and have the ability to lyse target cells (50). T regs, on the contrary, suppress antitumor immune response through the expression of CTLA-4 and the secretion of IL-10 and TGF-β, which contribute to further tumor growth (50). Our results suggest that the neoTx does not

directly increase the number of $CD8^+$ T cells but mediate a selective $FOXP3^+CD4^+$ Treg depletion, which causes a shrinkage of the whole $CD45^+$ and $CD4^+$ leucocytic populations. Consequently, the proportion of infiltrating $CD8^+$ T cells to the entire leucocytes increased from 20% to 40%. Therefore, the alleviation of Treg-mediated T cell suppression by neoTx results in the restoration of $CD8^+$ T cell density. The same observations were made by Shibuya et al., where the $CD8^+$/Treg ratio was significantly higher after treatment, mostly due to a notably less infiltration of treated tumors with $FOXP3^+$ Tregs (61, 66). The prevalence of Tregs significantly increases along the progression from low-grade PanIN to invasive carcinoma and the possibility to reverse this trend through neoadjuvant approaches constitutes a valuable opportunity for antitumor immunotherapy (89).

High numbers of $CD8^+$ T cells have been almost universally associated with enhanced prognosis including melanoma, breast, bladder, urothelial, ovarian, colorectal, prostatic and lung cancer (51, 52). Meanwhile, the association of Treg cell infiltration with patients´ poorer outcome has been subject of controversy (52, 90). In PCa, high density of $CD8^+$ T cells have shown to be correlated with enhanced disease-free and overall survival (62). In a later study, Ino et al. demonstrated that low counts of Tregs, together with high $CD8^+$ T cells were able to predict more accurately the prognosis of PCa patients (24). In breast cancer, strong presence of $CD8^+$ tumor infiltrating lymphocytes in the residual tumor after neoTx constitutes an independent prognostic factor for improved prognosis (91). Due to the smaller number of patients and the heterogeneity in neoTx regimes, we were not able to obtain a similar independent prognostic value for $CD8^+$ and Tregs but altogether, our data strongly suggest that, like in breast cancer, these cells could play a pivotal role on the prolonged survival after neoTx in PCa patients. The reduced number of MDSCs and Tregs after neoTx and the

strong correlation with $CD8^+$ T cells observed in our results, support the hypothesis that the antitumoral effect of chemotherapy relies on its capacity to selectively deplete immunosuppressive cells. Moreover, in contrast to breast and prostate cancer, the number of mitotic tumor cells was constant after neoTx in PCa (42, 44), which suggests that the direct cytotoxicity of chemotherapeutical agents on pancreatic tumor cells accounts merely for a minor role on its clinical benefit and seems to be subordinated to the immune cell mediated anti-tumor response.

However, Tregs are not the only cell-type involved in tumor-induced immunosuppression (8). Also, MDSCs have been identified as major modulators of tumor tolerance. Recent evidence demonstrated that gemcitabine and 5-FU induce a transient selective depletion of MDSCs, resulting in the enhancement of intratumoral $CD8^+$ T cell antitumor activity (8). The diminished number of MDSCs after neoTx and the strong correlation with $CD8^+$ T cells observed in our results, further supports the hypothesis that, beyond its direct tumor cytotoxicity, neoTx possesses immunogenic properties that rely on its capacity to selectively deplete immunosuppressive cells. NeoTx-mediated cancer cell death also enhances the antitumor response by the emission of "danger" and "eat me" signals by tumor cells that mediate their phagocytosis by DCs and results in increased activation and antigen-presenting potential of DCs (67, 85, 92). It has been reported that the molecular signals mediating this immunoadjuvant effect of neoTx consist in the expression of calreticuline on the cell surface together with the release of the HMGB1 protein by dying tumor cells, which can be recognized by the Toll-like receptor-4 (TLR4) on DCs (85). DCs present in the pancreatic tumor microenvironment have been proven deficient of the TLR4, and whether neoTx is able to alleviate the immune defect induced by deficient TLR4 signalling needs, however, further elucidation (93).

Contrary to our results, tumor infiltration by NK cells predicts a good prognosis in colorectal (93), gastric (94) and hepatocellular cancer (52, 95). In PCa, only the circulating NK cells on treatment-naive patients have been demonstrated to be linked to an increased overall survival (96). Studies evaluating the role of neoTx on NK cell infiltration are limited and show controversial results (96). We found a significant decrease in the density of intratumoral NK cells after neoTx, which was accompanied by enhanced clinical outcome. Recent reports about lung cancer reported an anergic phenotype of intratumoral NK, which renders them unable to secrete IFN-γ and to kill tumor cells (52). Similarly, a significant impairment in NK cells' cytotoxicity has been observed in PCa, as activating receptors such as NK group 2 member D (NKG2D), NKp30 and NKp46 are notably downregulated in PCa patients (50). We hypothesize that, intratumoral NK cells have an anergic phenotype, and that dysfunctional NK cells may represent a factor promoting tumor progression and may therefore be more susceptible to neoTx. However, whether the release of TGF-β and other cytokines by pancreatic tumor cells may be responsible for maintaining infiltrating NK cells in an anergic or even protumorigenic state needs further elucidation.

The effect of B cell infiltration in PCa is far from being elucidated. Mouse models of spontaneous cancers suggest an immunosuppressive role, possibly due to the production of IL10, which promotes an M2 phenotype in macrophages (52). Studies on breast cancer reported a possible metastasis-promoting role of B cells by converting resting $CD4^+$ T cells into Tregs (52). The amount of infiltrating B cells has been associated with good prognosis in some histological subtypes of breast and epithelial ovarian cancer (52), but studies analysing their potential as prognostic markers on many tumors are lacking. In our patient cohort, the density of B cells was not correlated with the overall survival and no change was observed in the number of tumor-infiltrating

B cells after neoTx. Nevertheless, intratumoral B cells constitute the most prevalent immune cell type after neoTx, probably due to an intrinsic chemoresistance and pronounced independence from the rest of intratumoral immune cell types, as they constitute the only cell population that is not correlated to any other immune cell type. Despite their intratumoral prevalence, our findings suggest that these cells play only a minor part in the immunological response of PCa to neoTx.

PCa is also infiltrated by tumor-associated macrophages, which have been associated with metastasis and poor prognosis in the majority of the investigated malignancies (24, 56, 57). Plasticity and diversity are the hallmarks of macrophages (87). Once circulating macrophages are recruited into the tumor microenvironment, they acquire either an antitumor M1-phenotype or the immunosuppressive M2-polarization (87). However, recent research demonstrated that the traditional M1- and M2-polarized macrophages are just both extremes of a continuum of functional states and that most of the intratumoral macrophages are in changeable status between M1 and M2 (87). According to these findings, neoTx has been reported to be able to redirect the polarization of macrophages into the antitumorigenic M1 phenotype, providing evidence that macrophages might develop an antitumorigenic role if properly educated by therapeutics (97). In our cohort, we also observed an increase of the intratumoral M1 macrophage infiltration after neoTx, but in contrast to the abovementioned study, the density of M2 macrophages remained unaltered (97). In both cases, the density of $CD68^+$ macrophages remained constant and did not correlate patients´ survival. However, the mechanisms of the enhanced antitumoral activity of macrophages after neoTx are still not clear. In vitro assays suggest that chemotherapeutical agents can exert their modulatory effect by acting directly on the macrophages, whereas the high

correlation between $CD8^+$ T cells and M1 macrophages in our study, implies the presence of an additional T-cell dependent modulatory effect.

Whether the immune context after neoTx is able to predict therapeutic responses is of paramount importance for the clinical management of PCa patients (52). Our results demonstrated that histopathological features like the desmoplastic reaction, NI and the intratumoral infiltration with $CD4^+$ T cells and NK cells could predict survival in a similar way to traditionally recognised prognostic factors like lymph node status, surgical margins and grade of differentiation. Unexpectedly, the tumor proliferation rate rose as the most potent prognostic marker for PCa with a survival benefit for patients with low mitotic rate of over 26 months. Ki67 is a simple, inexpensive method, which could be highly useful in the stratification of PCa patients and as a powerful prognostic factor (43). For this purpose, however, further validation studies showing an independent and reproducible prognostic potential are needed.

The main limitations of this study included its retrospective nature and potential selection bias for surgery as well as the heterogeneity of neoTx regimes and tumor characteristics. An ideal study with the same focus as ours should consider these limitations in a prospective design.

Conclusion

We performed the first and currently most comprehensive histopathological analysis that examined the role of neoTx on borderline resectable and locally advanced PCa and demonstrated the ability of neoTx to enrich anti-tumor immune cells in the tumor microenvironment. This effect is independent of the applied pre-treatment regimen and is characterized by selective depletion of Tregs and MDSCs, which may lead to

increased T cell antitumor activity. NeoTx exerted also a stromal-modulating effect by restraining the desmoplastic reaction and NI. Surprisingly, two of the most established mechanisms of tumorigenesis exhibited no change after therapy, in fact, both angiogenesis and the proliferation rate of tumor cells remained constant. Overall, we demonstrated a pronounced interrelationship between each of the components of the tumor microenvironment.

To conclude, we hereby demonstrate that the beneficial effect of neoTx may not rely, as traditionally believed, on the direct cytotoxicity of the chemotherapeutical agents, but on the restoration of the immune cell-mediated anti-tumor response. The possibility of combining traditional neoTx with immunotherapy may unleash long-term and more effective anti-tumoral immune responses, beneficially alter the multiple immune-stroma activating crosstalks, and eventually improve the prognosis of locally advanced PCa.

References

1. Kleeff J, Korc M, Apte M, La Vecchia C, Johnson CD, Biankin AV, Neale RE, Tempero M, Tuveson DA, Hruban RH, Neoptolemos JP. Pancreatic cancer. Nat Rev Dis Primers. 2016;2:16022.
2. McGuigan A, Kelly P, Turkington RC, Jones C, Coleman HG, McCain RS. Pancreatic cancer: A review of clinical diagnosis, epidemiology, treatment and outcomes. World J Gastroenterol. 2018;24(43):4846-61.
3. Vincent A, Herman J, Schulick R, Hruban RH, Goggins M. Pancreatic cancer. The Lancet. 2011;378(9791):607-20.
4. Feig C, Gopinathan A, Neesse A, Chan DS, Cook N, Tuveson DA. The pancreas cancer microenvironment. Clin Cancer Res. 2012;18(16):4266-76.
5. Kim J, Hoffman JP, Alpaugh RK, Rhim AD, Reichert M, Stanger BZ, Furth EE, Sepulveda AR, Yuan CX, Won KJ, Donahue G, Sands J, Gumbs AA, Zaret KS. An iPSC line from human pancreatic ductal adenocarcinoma undergoes early to invasive stages of pancreatic cancer progression. Cell Rep. 2013;3(6):2088-99.
6. Makohon-Moore A, Brosnan JA, Iacobuzio-Donahue CA. Pancreatic cancer genomics: insights and opportunities for clinical translation. Genome Med. 2013;5(3):26.
7. Iacobuzio-Donahue CA, Velculescu VE, Wolfgang CL, Hruban RH. Genetic basis of pancreas cancer development and progression: insights from whole-exome and whole-genome sequencing. Clin Cancer Res. 2012;18(16):4257-65.

8. Vincent J, Mignot G, Chalmin F, Ladoire S, Bruchard M, Chevriaux A, Martin F, Apetoh L, Rebe C, Ghiringhelli F. 5-Fluorouracil selectively kills tumor-associated myeloid-derived suppressor cells resulting in enhanced T cell-dependent antitumor immunity. Cancer Res. 2010;70(8):3052-61.
9. Schneider G, Siveke JT, Eckel F, Schmid RM. Pancreatic Cancer: Basic and Clinical Aspects. Gastroenterology. 2005;128(6):1606-25.
10. Esposito I, Konukiewitz B, Schlitter AM, Kloppel G. [New insights into the origin of pancreatic cancer. Role of atypical flat lesions in pancreatic carcinogenesis]. Pathologe. 2012;33 Suppl 2:189-93.
11. Rossi ML, Rehman AA, Gondi CS. Therapeutic options for the management of pancreatic cancer. World J Gastroenterol. 2014;20(32):11142-59.
12. Hruban RH, Goggins M, Parsons J, Kern SE. Progression model for pancreatic cancer. Clin Cancer Res. 2000;6(8):2969-72.
13. Kim VM, Ahuja N. Early detection of pancreatic cancer. Chin J Cancer Res. 2015;27(4):321-31.
14. Erkan M, Hausmann S, Michalski CW, Schlitter AM, Fingerle AA, Dobritz M, Friess H, Kleeff J. How fibrosis influences imaging and surgical decisions in pancreatic cancer. Front Physiol. 2012;3:389.
15. Rana SS, Bhasin DK, Sharma V, Rao C, Singh K. Role of endoscopic ultrasound in the diagnosis of pancreas divisum. Endosc Ultrasound. 2013;2(1):7-10.
16. Ergul N, Gundogan C, Tozlu M, Toprak H, Kadioglu H, Aydin M, Cermik TF. Role of (18)F-fluorodeoxyglucose positron emission tomography/computed tomography in diagnosis and management of pancreatic cancer; comparison with multidetector row computed tomography, magnetic resonance imaging and endoscopic ultrasonography. Rev Esp Med Nucl Imagen Mol. 2014;33(3):159-64.
17. Katz MH, Marsh R, Herman JM, Shi Q, Collison E, Venook AP, Kindler HL, Alberts SR, Philip P, Lowy AM, Pisters PW, Posner MC, Berlin JD, Ahmad SA. Borderline resectable pancreatic cancer: need for standardization and methods for optimal clinical trial design. Ann Surg Oncol. 2013;20(8):2787-95.
18. Zhan HX, Xu JW, Wu D, Wu ZY, Wang L, Hu SY, Zhang GY. Neoadjuvant therapy in pancreatic cancer: a systematic review and meta-analysis of prospective studies. Cancer Med. 2017;6(6):1201-19.
19. Rahman SH, Urquhart R, Molinari M. Neoadjuvant therapy for resectable pancreatic cancer. World J Gastrointest Oncol. 2017;9(12):457-65.
20. Heinrich S. Neoadjuvant therapy for pancreatic ductal adenocarcinoma-real effects or patient selection? Hepatobiliary Surg Nutr. 2018;7(4):289-91.
21. Zhang W, Tian H, Yang SH. The Efficacy of Neoadjuvant Chemotherapy for HER-2-Positive Locally Advanced Breast Cancer and Survival Analysis. Anal Cell Pathol (Amst). 2017;2017:1350618.
22. Conroy T, Desseigne F, Ychou M, Bouche O, Guimbaud R, Becouarn Y, Adenis A, Raoul JL, Gourgou-Bourgade S, de la Fouchardiere C, Bennouna J, Bachet JB, Khemissa-Akouz F, Pere-Verge D, Delbaldo C, Assenat E, Chauffert B, Michel P, Montoto-Grillot C, Ducreux M, Groupe Tumeurs Digestives of U, Intergroup P. FOLFIRINOX versus gemcitabine for metastatic pancreatic cancer. N Engl J Med. 2011;364(19):1817-25.
23. Seiler C, Gillen S, Schuster T, Meyer zum Büschenfelde C, Friess H, Kleeff J. Preoperative/Neoadjuvant Therapy in Pancreatic Cancer: A Systematic Review and Meta-analysis of Response and Resection Percentages. PLoS Medicine. 2010;7(4).
24. Ino Y, Yamazaki-Itoh R, Shimada K, Iwasaki M, Kosuge T, Kanai Y, Hiraoka N. Immune cell infiltration as an indicator of the immune microenvironment of pancreatic cancer. Br J Cancer. 2013;108(4):914-23.

25. Pietras K, Ostman A. Hallmarks of cancer: interactions with the tumor stroma. Exp Cell Res. 2010;316(8):1324-31.
26. Apte MV, Xu Z, Pothula S, Goldstein D, Pirola RC, Wilson JS. Pancreatic cancer: The microenvironment needs attention too! Pancreatology. 2015;15(4 Suppl):S32-8.
27. Dougan SK. The Pancreatic Cancer Microenvironment. Cancer J. 2017;23(6):321-5.
28. Erkan M, Michalski CW, Rieder S, Reiser-Erkan C, Abiatari I, Kolb A, Giese NA, Esposito I, Friess H, Kleeff J. The activated stroma index is a novel and independent prognostic marker in pancreatic ductal adenocarcinoma. Clin Gastroenterol Hepatol. 2008;6(10):1155-61.
29. Ozdemir BC, Pentcheva-Hoang T, Carstens JL, Zheng X, Wu CC, Simpson TR, Laklai H, Sugimoto H, Kahlert C, Novitskiy SV, De Jesus-Acosta A, Sharma P, Heidari P, Mahmood U, Chin L, Moses HL, Weaver VM, Maitra A, Allison JP, LeBleu VS, Kalluri R. Depletion of carcinoma-associated fibroblasts and fibrosis induces immunosuppression and accelerates pancreas cancer with reduced survival. Cancer Cell. 2014;25(6):719-34.
30. Bever KM, Sugar EA, Bigelow E, Sharma R, Laheru D, Wolfgang CL, Jaffee EM, Anders RA, De Jesus-Acosta A, Zheng L. The prognostic value of stroma in pancreatic cancer in patients receiving adjuvant therapy. HPB (Oxford). 2015;17(4):292-8.
31. Miyashita T, Tajima H, Makino I, Okazaki M, Yamaguchi T, Ohbatake Y, Nakanuma S, Hayashi H, Takamura H, Ninomiya I, Fushida S, Kishimoto K, Harmon JW, Ohta T. Neoadjuvant Chemotherapy with Gemcitabine Plus Nab-paclitaxel Reduces the Number of Cancer-associated Fibroblasts Through Depletion of Pancreatic Stroma. Anticancer Res. 2018;38(1):337-43.
32. Ene-Obong A, Clear AJ, Watt J, Wang J, Fatah R, Riches JC, Marshall JF, Chin-Aleong J, Chelala C, Gribben JG, Ramsay AG, Kocher HM. Activated pancreatic stellate cells sequester CD8+ T cells to reduce their infiltration of the juxtatumoral compartment of pancreatic ductal adenocarcinoma. Gastroenterology. 2013;145(5):1121-32.
33. Carstens JL, Correa de Sampaio P, Yang D, Barua S, Wang H, Rao A, Allison JP, LeBleu VS, Kalluri R. Spatial computation of intratumoral T cells correlates with survival of patients with pancreatic cancer. Nat Commun. 2017;8:15095.
34. Erkan M, Reiser-Erkan C, Michalski CW, Deucker S, Sauliunaite D, Streit S, Esposito I, Friess H, Kleeff J. Cancer-Stellate Cell Interactions Perpetuate the Hypoxia-Fibrosis Cycle in Pancreatic Ductal Adenocarcinoma. Neoplasia. 2009;11(5):497-508.
35. Longo V, Brunetti O, Gnoni A, Cascinu S, Gasparini G, Lorusso V, Ribatti D, Silvestris N. Angiogenesis in pancreatic ductal adenocarcinoma: A controversial issue. Oncotarget. 2016;7(36):58649-58.
36. van der Zee JA, van Eijck CH, Hop WC, van Dekken H, Dicheva BM, Seynhaeve AL, Koning GA, Eggermont AM, ten Hagen TL. Angiogenesis: a prognostic determinant in pancreatic cancer? Eur J Cancer. 2011;47(17):2576-84.
37. Demir IE, Ceyhan GO, Liebl F, D'Haese JG, Maak M, Friess H. Neural invasion in pancreatic cancer: the past, present and future. Cancers (Basel). 2010;2(3):1513-27.
38. Demir IE, Ceyhan GO, Rauch U, Altintas B, Klotz M, Muller MW, Buchler MW, Friess H, Schafer KH. The microenvironment in chronic pancreatitis and pancreatic cancer induces neuronal plasticity. Neurogastroenterol Motil. 2010;22(4):480-90, e112-3.

39. Bapat AA, Hostetter G, Von Hoff DD, Han H. Perineural invasion and associated pain in pancreatic cancer. Nat Rev Cancer. 2011;11(10):695-707.
40. Ceyhan GO, Bergmann F, Kadihasanoglu M, Altintas B, Demir IE, Hinz U, Muller MW, Giese T, Buchler MW, Giese NA, Friess H. Pancreatic neuropathy and neuropathic pain--a comprehensive pathomorphological study of 546 cases. Gastroenterology. 2009;136(1):177-86 e1.
41. Liang D, Shi S, Xu J, Zhang B, Qin Y, Ji S, Xu W, Liu J, Liu L, Liu C, Long J, Ni Q, Yu X. New insights into perineural invasion of pancreatic cancer: More than pain. Biochim Biophys Acta. 2016;1865(2):111-22.
42. Ghanim B, Klikovits T, Hoda MA, Lang G, Szirtes I, Setinek U, Rozsas A, Renyi-Vamos F, Laszlo V, Grusch M, Filipits M, Scheed A, Jakopovic M, Samarzija M, Brcic L, Stancic-Rokotov D, Kern I, Rozman A, Dekan G, Klepetko W, Berger W, Glasz T, Dome B, Hegedus B. Ki67 index is an independent prognostic factor in epithelioid but not in non-epithelioid malignant pleural mesothelioma: a multicenter study. Br J Cancer. 2015;112(5):783-92.
43. Ciancio N, Galasso MG, Campisi R, Bivona L, Migliore M, Di Maria GU. Prognostic value of p53 and Ki67 expression in fiberoptic bronchial biopsies of patients with non small cell lung cancer. Multidiscip Respir Med. 2012;7(1):29.
44. Tretiakova MS, Wei W, Boyer HD, Newcomb LF, Hawley S, Auman H, Vakar-Lopez F, McKenney JK, Fazli L, Simko J, Troyer DA, Hurtado-Coll A, Thompson IM, Jr., Carroll PR, Ellis WJ, Gleave ME, Nelson PS, Lin DW, True LD, Feng Z, Brooks JD. Prognostic value of Ki67 in localized prostate carcinoma: a multi-institutional study of >1000 prostatectomies. Prostate Cancer Prostatic Dis. 2016;19(3):264-70.
45. Kim H, Park CY, Lee JH, Kim JC, Cho C-K, Kim HJ. Ki-67 and p53 expression as a predictive marker for early postoperative recurrence in pancreatic head cancer. Annals of Surgical Treatment and Research. 2015;88(4).
46. Stanton KJ, Sidner RA, Miller GA, Cummings OW, Schmidt CM, Howard TJ, Wiebke EA. Analysis of Ki-67 antigen expression, DNA proliferative fraction, and survival in resected cancer of the pancreas. The American Journal of Surgery. 2003;186(5):486-92.
47. Martinez-Bosch N, Vinaixa J, Navarro P. Immune Evasion in Pancreatic Cancer: From Mechanisms to Therapy. Cancers (Basel). 2018;10(1).
48. Neesse A, Algul H, Tuveson DA, Gress TM. Stromal biology and therapy in pancreatic cancer: a changing paradigm. Gut. 2015;64(9):1476-84.
49. Pillarisetty VG. The pancreatic cancer microenvironment: an immunologic battleground. Oncoimmunology. 2014;3(8):e950171.
50. Chang JH, Jiang Y, Pillarisetty VG. Role of immune cells in pancreatic cancer from bench to clinical application: An updated review. Medicine (Baltimore). 2016;95(49):e5541.
51. McCoy MJ, Hemmings C, Miller TJ, Austin SJ, Bulsara MK, Zeps N, Nowak AK, Lake RA, Platell CF. Low stromal Foxp3+ regulatory T-cell density is associated with complete response to neoadjuvant chemoradiotherapy in rectal cancer. Br J Cancer. 2015;113(12):1677-86.
52. Fridman WH, Pages F, Sautes-Fridman C, Galon J. The immune contexture in human tumours: impact on clinical outcome. Nat Rev Cancer. 2012;12(4):298-306.
53. Foucher ED, Ghigo C, Chouaib S, Galon J, Iovanna J, Olive D. Pancreatic Ductal Adenocarcinoma: A Strong Imbalance of Good and Bad Immunological Cops in the Tumor Microenvironment. Front Immunol. 2018;9:1044.
54. Hanke N, Alizadeh D, Katsanis E, Larmonier N. Dendritic cell tumor killing activity and its potential applications in cancer immunotherapy. Crit Rev Immunol. 2013;33(1):1-21.

55. Pergamo M, Miller G. Myeloid-derived suppressor cells and their role in pancreatic cancer. Cancer Gene Ther. 2017;24(3):100-5.
56. Kurahara H, Shinchi H, Mataki Y, Maemura K, Noma H, Kubo F, Sakoda M, Ueno S, Natsugoe S, Takao S. Significance of M2-polarized tumor-associated macrophage in pancreatic cancer. J Surg Res. 2011;167(2):e211-9.
57. Protti MP, De Monte L. Immune infiltrates as predictive markers of survival in pancreatic cancer patients. Front Physiol. 2013;4:210.
58. Eriksson E, Wenthe J, Irenaeus S, Loskog A, Ullenhag G. Gemcitabine reduces MDSCs, tregs and TGFβ-1 while restoring the teff/treg ratio in patients with pancreatic cancer. Journal of Translational Medicine. 2016;14(1).
59. Josefowicz SZ, Lu LF, Rudensky AY. Regulatory T cells: mechanisms of differentiation and function. Annu Rev Immunol. 2012;30:531-64.
60. Jang JE, Hajdu CH, Liot C, Miller G, Dustin ML, Bar-Sagi D. Crosstalk between Regulatory T Cells and Tumor-Associated Dendritic Cells Negates Anti-tumor Immunity in Pancreatic Cancer. Cell Rep. 2017;20(3):558-71.
61. Tsuchikawa T, Takeuchi S, Nakamura T, Shichinohe T, Hirano S. Clinical impact of chemotherapy to improve tumor microenvironment of pancreatic cancer. World J Gastrointest Oncol. 2016;8(11):786-92.
62. Tsujikawa T, Kumar S, Borkar RN, Azimi V, Thibault G, Chang YH, Balter A, Kawashima R, Choe G, Sauer D, El Rassi E, Clayburgh DR, Kulesz-Martin MF, Lutz ER, Zheng L, Jaffee EM, Leyshock P, Margolin AA, Mori M, Gray JW, Flint PW, Coussens LM. Quantitative Multiplex Immunohistochemistry Reveals Myeloid-Inflamed Tumor-Immune Complexity Associated with Poor Prognosis. Cell Rep. 2017;19(1):203-17.
63. Gupta A, Probst HC, Vuong V, Landshammer A, Muth S, Yagita H, Schwendener R, Pruschy M, Knuth A, van den Broek M. Radiotherapy promotes tumor-specific effector CD8+ T cells via dendritic cell activation. J Immunol. 2012;189(2):558-66.
64. Lin HJ, Lin J. Seed-in-Soil: Pancreatic Cancer Influenced by Tumor Microenvironment. Cancers (Basel). 2017;9(7).
65. Pylayeva-Gupta Y, Das S, Handler JS, Hajdu CH, Coffre M, Koralov SB, Bar-Sagi D. IL35-Producing B Cells Promote the Development of Pancreatic Neoplasia. Cancer Discov. 2016;6(3):247-55.
66. Shibuya KC, Goel VK, Xiong W, Sham JG, Pollack SM, Leahy AM, Whiting SH, Yeh MM, Yee C, Riddell SR, Pillarisetty VG. Pancreatic ductal adenocarcinoma contains an effector and regulatory immune cell infiltrate that is altered by multimodal neoadjuvant treatment. PLoS One. 2014;9(5):e96565.
67. Homma Y, Taniguchi K, Murakami T, Nakagawa K, Nakazawa M, Matsuyama R, Mori R, Takeda K, Ueda M, Ichikawa Y, Tanaka K, Endo I. Immunological impact of neoadjuvant chemoradiotherapy in patients with borderline resectable pancreatic ductal adenocarcinoma. Ann Surg Oncol. 2014;21(2):670-6.
68. Parra ER, Villalobos P, Behrens C, Jiang M, Pataer A, Swisher SG, William WN, Jr., Zhang J, Lee J, Cascone T, Heymach JV, Forget MA, Haymaker C, Bernatchez C, Kalhor N, Weissferdt A, Moran C, Zhang J, Vaporciyan A, Gibbons DL, Sepesi B, Wistuba, II. Effect of neoadjuvant chemotherapy on the immune microenvironment in non-small cell lung carcinomas as determined by multiplex immunofluorescence and image analysis approaches. J Immunother Cancer. 2018;6(1):48.
69. von Ahrens D, Bhagat TD, Nagrath D, Maitra A, Verma A. The role of stromal cancer-associated fibroblasts in pancreatic cancer. J Hematol Oncol. 2017;10(1):76.
70. Watt J, Kocher HM. The desmoplastic stroma of pancreatic cancer is a barrier to immune cell infiltration. Oncoimmunology. 2013;2(12):e26788.

71. Rhim AD, Oberstein PE, Thomas DH, Mirek ET, Palermo CF, Sastra SA, Dekleva EN, Saunders T, Becerra CP, Tattersall IW, Westphalen CB, Kitajewski J, Fernandez-Barrena MG, Fernandez-Zapico ME, Iacobuzio-Donahue C, Olive KP, Stanger BZ. Stromal elements act to restrain, rather than support, pancreatic ductal adenocarcinoma. Cancer Cell. 2014;25(6):735-47.
72. Ohlund D, Handly-Santana A, Biffi G, Elyada E, Almeida AS, Ponz-Sarvise M, Corbo V, Oni TE, Hearn SA, Lee EJ, Chio, II, Hwang CI, Tiriac H, Baker LA, Engle DD, Feig C, Kultti A, Egeblad M, Fearon DT, Crawford JM, Clevers H, Park Y, Tuveson DA. Distinct populations of inflammatory fibroblasts and myofibroblasts in pancreatic cancer. J Exp Med. 2017;214(3):579-96.
73. Apte MV, Wilson JS, Lugea A, Pandol SJ. A starring role for stellate cells in the pancreatic cancer microenvironment. Gastroenterology. 2013;144(6):1210-9.
74. Demir IE, Friess H, Ceyhan GO. Nerve-cancer interactions in the stromal biology of pancreatic cancer. Front Physiol. 2012;3:97.
75. Chatterjee D, Katz MH, Rashid A, Wang H, Iuga AC, Varadhachary GR, Wolff RA, Lee JE, Pisters PW, Crane CH, Gomez HF, Abbruzzese JL, Fleming JB, Wang H. Perineural and intraneural invasion in posttherapy pancreaticoduodenectomy specimens predicts poor prognosis in patients with pancreatic ductal adenocarcinoma. Am J Surg Pathol. 2012;36(3):409-17.
76. Ceyhan GO, Demir IE, Rauch U, Bergmann F, Muller MW, Buchler MW, Friess H, Schafer KH. Pancreatic neuropathy results in "neural remodeling" and altered pancreatic innervation in chronic pancreatitis and pancreatic cancer. Am J Gastroenterol. 2009;104(10):2555-65.
77. Vonlaufen A, Joshi S, Qu C, Phillips PA, Xu Z, Parker NR, Toi CS, Pirola RC, Wilson JS, Goldstein D, Apte MV. Pancreatic stellate cells: partners in crime with pancreatic cancer cells. Cancer Res. 2008;68(7):2085-93.
78. Stopczynski RE, Normolle DP, Hartman DJ, Ying H, DeBerry JJ, Bielefeldt K, Rhim AD, DePinho RA, Albers KM, Davis BM. Neuroplastic changes occur early in the development of pancreatic ductal adenocarcinoma. Cancer Res. 2014;74(6):1718-27.
79. Lagarde SM, Phillips AW, Navidi M, Disep B, Immanuel A, Griffin SM. The presence of lymphovascular and perineural infiltration after neoadjuvant therapy and oesophagectomy identifies patients at high risk for recurrence. Br J Cancer. 2015;113(10):1427-33.
80. Liebl F, Demir IE, Mayer K, Schuster T, D'Haese JG, Becker K, Langer R, Bergmann F, Wang K, Rosenberg R, Novotny AR, Feith M, Reim D, Friess H, Ceyhan GO. The impact of neural invasion severity in gastrointestinal malignancies: a clinicopathological study. Ann Surg. 2014;260(5):900-7; discussion 7-8.
81. Takahashi H, Ohigashi H, Ishikawa O, Gotoh K, Yamada T, Nagata S, Tomita Y, Eguchi H, Doki Y, Yano M. Perineural invasion and lymph node involvement as indicators of surgical outcome and pattern of recurrence in the setting of preoperative gemcitabine-based chemoradiation therapy for resectable pancreatic cancer. Ann Surg. 2012;255(1):95-102.
82. Rosenberg A, Mahalingam D. Immunotherapy in pancreatic adenocarcinoma-overcoming barriers to response. J Gastrointest Oncol. 2018;9(1):143-59.
83. Songchuan Guo MC, George Miller, Lawrence Leichman, Jennifer Wu. Immunotherapy in pancreatic cancer: Unleash its potential through novel combinations. World Journal of Clinical Oncology. 2017;8(3):230-40.
84. Liu J, Blake SJ, Yong MC, Harjunpaa H, Ngiow SF, Takeda K, Young A, O'Donnell JS, Allen S, Smyth MJ, Teng MW. Improved Efficacy of Neoadjuvant Compared to Adjuvant Immunotherapy to Eradicate Metastatic Disease. Cancer Discov. 2016;6(12):1382-99.

85. Apetoh L, Ghiringhelli F, Tesniere A, Obeid M, Ortiz C, Criollo A, Mignot G, Maiuri MC, Ullrich E, Saulnier P, Yang H, Amigorena S, Ryffel B, Barrat FJ, Saftig P, Levi F, Lidereau R, Nogues C, Mira JP, Chompret A, Joulin V, Clavel-Chapelon F, Bourhis J, Andre F, Delaloge S, Tursz T, Kroemer G, Zitvogel L. Toll-like receptor 4-dependent contribution of the immune system to anticancer chemotherapy and radiotherapy. Nat Med. 2007;13(9):1050-9.
86. Robert C. Is earlier better for melanoma checkpoint blockade? Nat Med. 2018;24(11):1645-8.
87. Liu Q, Liao Q, Zhao Y. Chemotherapy and tumor microenvironment of pancreatic cancer. Cancer Cell Int. 2017;17:68.
88. Dunn GP, Old LJ, Schreiber RD. The three Es of cancer immunoediting. Annu Rev Immunol. 2004;22:329-60.
89. Hiraoka N, Onozato K, Kosuge T, Hirohashi S. Prevalence of FOXP3+ regulatory T cells increases during the progression of pancreatic ductal adenocarcinoma and its premalignant lesions. Clin Cancer Res. 2006;12(18):5423-34.
90. Tang SC, Chen YC. Novel therapeutic targets for pancreatic cancer. World J Gastroenterol. 2014;20(31):10825-44.
91. Al-Saleh K, Abd El-Aziz N, Ali A, Abozeed W, Abd El-Warith A, Ibraheem A, Ansari J, Al-Rikabi A, Husain S, Nabholtz JM. Predictive and prognostic significance of CD8(+) tumor-infiltrating lymphocytes in patients with luminal B/HER 2 negative breast cancer treated with neoadjuvant chemotherapy. Oncol Lett. 2017;14(1):337-44.
92. Menard C, Ghiringhelli F, Roux S, Chaput N, Mateus C, Grohmann U, Caillat-Zucman S, Zitvogel L, Robert C. CTLA-4 Blockade Confers Lymphocyte Resistance to Regulatory T-Cells in Advanced Melanoma: Surrogate Marker of Efficacy of Tremelimumab? Clinical Cancer Research. 2008;14(16):5242-9.
93. Coca S, Perez-Piqueras J, Martinez D, Colmenarejo A, Saez MA, Vallejo C, Martos JA, Moreno M. The prognostic significance of intratumoral natural killer cells in patients with colorectal carcinoma. Cancer. 1997;79(12):2320-8.
94. Ishigami S, Natsugoe S, Tokuda K, Nakajo A, Che X, Iwashige H, Aridome K, Hokita S, Aikou T. Prognostic value of intratumoral natural killer cells in gastric carcinoma. Cancer. 2000;88(3):577-83.
95. Zhao JJ, Pan QZ, Pan K, Weng DS, Wang QJ, Li JJ, Lv L, Wang DD, Zheng HX, Jiang SS, Zhang XF, Xia JC. Interleukin-37 mediates the antitumor activity in hepatocellular carcinoma: role for CD57+ NK cells. Sci Rep. 2014;4:5177.
96. Davis M, Conlon K, Bohac GC, Barcenas J, Leslie W, Watkins L, Lamzabi I, Deng Y, Li Y, Plate JM. Effect of pemetrexed on innate immune killer cells and adaptive immune T cells in subjects with adenocarcinoma of the pancreas. J Immunother. 2012;35(8):629-40.
97. Di Caro G, Cortese N, Castino GF, Grizzi F, Gavazzi F, Ridolfi C, Capretti G, Mineri R, Todoric J, Zerbi A, Allavena P, Mantovani A, Marchesi F. Dual prognostic significance of tumour-associated macrophages in human pancreatic adenocarcinoma treated or untreated with chemotherapy. Gut. 2016;65(10):1710-20.

Acknowledgments

First of all, I would like to thank my mentor I. Ekin Demir for unconditionally supporting me over these years and for always understanding me, even when I couldn´t. His motivation and fascination for research have profoundly inspired me for this thesis and continue inspiring me every day. Thank you for encouraging my research and for allowing me to grow as a research scientist, it was a privilege and an honor working for you!

I would also like to mention Prof. Güralp O. Ceyhan, he gave me the freedom to build my thesis as my own work but had the ability to guide me and steered me in the right direction whenever he thought I needed it. Also, thank you to Prof. Helmut Friess, because he gave me the opportunity to join his team and encouraged me in every step of my research career.

I would also like to thank Steffen Teller and Ulrike Bourquain for always been willing to help me find a solution and for their enormous support in all technical aspects of this thesis.

I thank my fellow labmates for the mutual motivation, for the weekends we spend together on the lab and for all the fun we have had in the last four years.

I would also like to thank Dr. Muckenhuber, Dr. Konukiewitz and Prof. Weichert, the pathologist who were involved in the histopathological analysis and helped me select the appropriate sections. Without their participation and input, the study could not have been successfully conducted

I would like to thank Till Slawik for his understanding and his patience on the hard days and for making me feel at home in a foreign country.

Last but not least, I would like to express my deepest gratitude to my parents, my family and my closest friends. This dissertation would have not been possible without their unfailing support, continued patience and warming words. Sincerely thank you.